MAGNETIC SEPARATION OF STRONGLY MAGNETIC PARTICLES USING ALTERNATING FIELD

by

OLUFEMI W. GOODLUCK.

A thesis submitted to the Faculty of Graduate Studies and Research in partial fulfillment of the requirements for the Degree of Master of Engineering.

Department of Mining and Metallurgical Engineering
McGill university
Montreal, Canada

ABSTRACT

An A-C demagnetizing solenoid has been used as a high gradient magnetic separator. Tests were conducted with synthetic mixtures of fine magnetite and silica.

The grade of magnetic product for the a.c. magnetic separator was compared with that obtained on a d.c. magnetic separator. Both separators were operated at the same magnetic field, H = 0.06 Tesla and slurry flowrate velocity of 0.03m/s.

The a.c. hgms produced a higher grade than the d.c. hgms. for all tested conditions. The reason for the higher grade in the a.c. hgms has been attributed to the effect of vibration induced on the particles by the magnetic forces associated with the alternating magnetic field. The vibration caused nonmagnetic particles to be shaken free and carried away by the fluid (water).

The application of an external mechanical vibrator in the d.c. hgms, resulted in an even greater improvement in grade. This supported the hypothesis regarding the role of vibration in magnetic separation.

A model capable of predicting the grade of magnetic product, has been postulated and successfully tested with the acquired test data.

RESUMÉ

Utilisant un solénoïde démagnétisant sur courant alternatif, comme séparateur magnétique à haut gradient (SMHG), des tests furent exécutés employant des mélanges synthétiques de fines particules de magnétite et de silice.

La teneur du produit magnétique pour le séparateur sur courant alternatif fut comparée à celle obtenue par un séparateur sur courant continu. Les deux unités produisant le même champ magnétique , soit H = 0.06 Tesla, et la pulpe étant alimentée a la vitesse de 0.03 m/s..

Le SMHG sur courant alternatif a obtenu des teneurs superieures à celles du SMHG sur courant continu et ce pour tous les tests. Le pourquoi de cette supériorite du SMHG sur courant alternatif tient de l'effet de vibration transmis aux particules par les forces magnétiques associés au champ sur courant alternatif. Cette vibration fait en sorte que les particules non-magnétiques prisionnières des magnétiques sont libérées puis évacuées par le fluide (eau).

L'utilisation d'un mécanisme externe de vibration associé au SMHG sur courant continu résulta en une amélioration dépassant la teneur du produit magnétique du SMHG sur courant alternatif, supportant ainsi l'hypothese émise sur le rôle de la vibration lors de la séparation magnétique.

Un modèle capable de prédire la teneur du produit magnétique (GM) fut avancé et appliqué avec succès sur des résultats pré-acquis.

ACKNOWLEDGEMENT

The author wishes to sincerely thank his supervisor, Professor J.A. Finch for his idea of the experiment, financial support and enthusiasm throughout the research program. Michel Leroux, for his constant assistanceship in the plumbing work, taking of measurements and obtaining an elusive magnetite sample. To Dr. R. S. Rao for the assaying of the zinc plant residues; I extend my appreciation.

Thanks to Maurice Beaunault and Mark Readman for their remarkable discussion on the electrical engineering aspect of this thesis.

To all my colleagues in the mineral processing group 1983-1985, with whom I had the joy of sharing the friendship and academic ideas - my salute and thanks for everything.

To my parents, relatives and friends in Nigeria for constant support, I am most grateful.

As well, I thank all Nigerians by way of the scholarship offered me for this course through the Nigerian Government.

TABLE OF CONTENTS

NOMENCLATURE

A	mass ratio of nonmags to mags in the feed.
a	probability of nonmags retention per unit A.
B	magnetic flux density.
b	particle radius.
D	demagnetizing factor.
db	element of magnetic flux density.
de	element change in energy stored.
df	element of phase angle.
dH/dx	magnetic field gradient.
dx	element of length of solenoid.
E	energy stored per particle.
e	porosity of suspension.
F	flocculation forces.
Fa.c.	magnetic force in demagnetizing solenoid.
Fc	competing forces.
Fd	hydrodynamic forces.
Fi	interparticle forces.
Fm	magnetic force.
f	phase angle.
Fv	fraction of volume fraction of voids, Uv.
fv	maximum fraction of Uv.
g	gravitational acceleration.
Gm	grade of magnetic product.
Gm	minimum grade of magnetic product.
H	magnetic field intensity.

Ha.c.	field intensity in demagnetizing solenoid.
Hd.c.	field intensity in electromagnetic coil.
Hm	magnitude of field intensity.
I	current in solenoid.
Ia.c.	alternating current.
Id.c.	direct current.
Im	magnitude of current.
i	instantaneous current.
k	volume suspectibility.
k'	proportionality constant.
L	total solenoid length.
L	slab thickness.
Mp	particle magnetization.
m	mass of particle.
μ_o	permeability of free space.
N	total number of wire turns on solenoid.
N	number of particles.
p	density of particle.
Pm	density of magnetite.
Ps	density of silica.
Rm	recovery of mags.
Rnm	recovery of nonmags.
r	interparticle distance.
r1	radius of solenoid.
η	fluid viscosity.
t	time.

V	volume of particle
v	relative velocity of particle to fluid.
$V_{a.c.}$	alternating current voltage.
$V_{d.c.}$	direct current voltage.
v	instantaneous voltage.
V_m	maximum voltage.
γ_v	volume fraction of voids.
w	angular velocity.
Z_m	magnitude of coil impedance.

LIST OF FIGURES

LIST OF TABLES.

AIM OF THESIS

Magnetic products from magnetic separators are usually contaminated with non-magnetic particles. These are entrapped physically among the magnetic particles. Kelland et al (1) recently demonstrated that an alternating current powered high gradient magnetic separator (a.c. hgms) gave higher grades of magnetite than a direct current powered (d.c. hgms) in magnetite/coal separation. No explanation was given.

It is the aim of this thesis to test this observation regarding a.c. hgms and explore possible reasons.

1. INTRODUCTION AND BACKGROUND THEORY

1.1 CONCEPT AND SOME APPLICATIONS OF MAGNETIC SEPARATION.

Magnetic separation techniques in mineral benefication have been long applied to achieve physical separation of minerals by exploiting differences in magnetic susceptibility of individual minerals. In recent years, the development of magnetic separators has recognized the importance of high field strength in polarizing feebly magnetic materials and the importance of magnetic gradients in developing magnetic forces in dipolar materials.

There are two general categories of magnetic separator used for mineral benefication - low intensity and high intensity. Both forms can be operated dry or wet. Low intensity magnetic separators (LIMS) are used, for example, as conveyor guard magnets to remove tramp iron from nonmagnetic ores, and for extracting strongly magnetic particles such as magnetite, and pyrrhotite (2). Another important area of use is for recovery of the magnetic heavy medium in coal washery plants (3,4) and in the concentration of some industrial minerals and base metal ores (5).

High intensity magnetic separation (HIMS) and high gradient magnetic separation (HGMS) are usually applied to achieve separation of a) mixtures containing a small proportion of strongly magnetic particles of fine size range <1 to minus 100um and b) mixtures of weakly magnetic particles of wide size range (6). The high intensity/high

gradient magnetic separation devices are used industrially in kaolin clay processing for removal of fine magnetic particles to improve clay brightness (7,8) in the concentration of fine iron-ore (hematite) and for upgrading of wolframite concentrates (9-11). Laboratory/pilot scale studies include treatment of leach residues for upgrading of precious metal content (12-14) and desulphurization of coal (15,16). An innovative application of hgms is in the separation of blood (17). Another application is filtration, for example, in the steel industry for removal of iron and iron oxides from the process water (18) and in power plants for removal of corrosion products (19).

The 1940s marked the beginning of commercial introduction of high intensity magnetic separators and over the years several different types were developed (5) such as the Jones HIMS, the Kolm-Marston HGMS and recently superconducting magnets. A full description of these devices has been given by Oberteuffer, and Hopstock and Lawver (20,21). Therefore, only a summary is presented here.

Jones HIMS device: The cyclic is shown in Figure 1 and was first patented by George H. Jones (22,9,23). The basic design principle is for the field to be at right angles to the flow. The matrix, made of grooved ferromagnetic plate, is placed in between the poles of an electromagnet. With the magnetic field applied, the feed, either wet or dry, passes through the matrix. The magnetic particles are captured on the surface of the matrix, and the

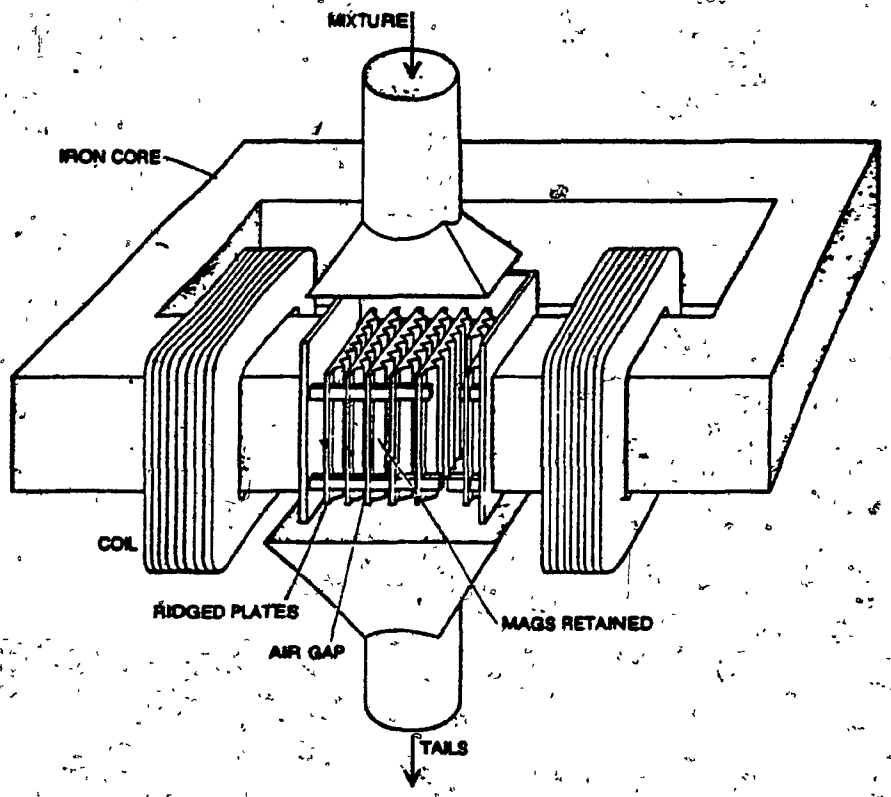

Figure 1 A Cyclic Matrix-Type Magnetic Separator.

nonmagnetic particles pass through. When the matrix is loaded the magnetic products are washed from the matrix with the electromagnet switched off.

A continous rotary separator which functions similarly to the cyclic device, developed for large scale operations is shown in Figure 2. The ferromagnetic matrix is mounted in an annular ring (carousel) which rotates through the magnetic field. The feeding and capturing of magnetic materials occur when the matrix is within the magnetic field. The nonmagnetics pass through into a launder while the magnetics are flushed into another launder when the matrix is out of the magnetic field.

The Kolm-Marston Separator (HGMS) (24-26): This device is similar to the Jones separator except the magnetic field and the flow are parallel. Both cyclic (batch) and continuous devices are available, figure 3.

The matrix is of steel wool or an expanded metal. In the continous device, the matrix is fitted in an annular ring, which rotates through the magnet heads. The magnet head is an elongated iron bound solenoid the coils of which have been turned up at both ends to enable the ring to pass through. The slurry is passed through openings in the magnet head. The nonmagnetics pass through while the magnetics are captured on the matrix and carried out of the magnetic field by the rotation of the annular ring to be discharged at the flush station.

The difference between HGMS and HIMS is that the

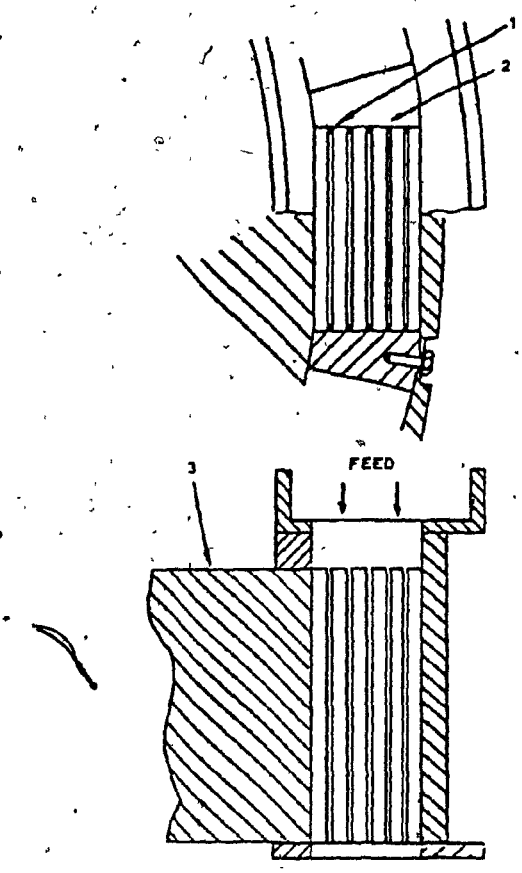

Platebox.

(1) Plate
(2) Brass strip
(3) Rotating disc

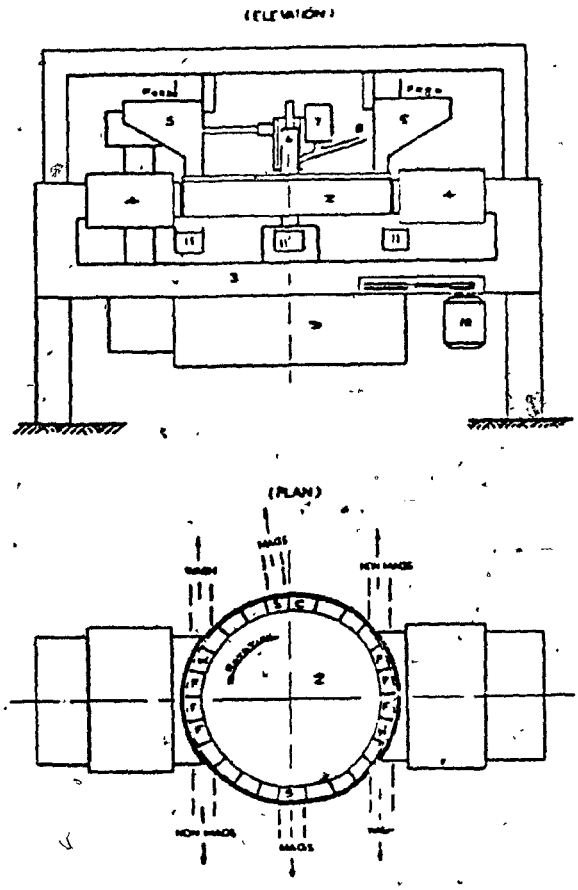

Arrangement of rotary separator.

(1) Platebox
(2) Rotating disc
(3) Magnet
(4) Permanent magnet on coils
(5) Feed hoppers
(6) Scour mechanism
(7) Air vessel
(8) Scour water pipe
(9) Gearbox
(10) Driving motor
(11) Launders

Figure 2 The Continuous Cyclic Matrix-Type Separator.

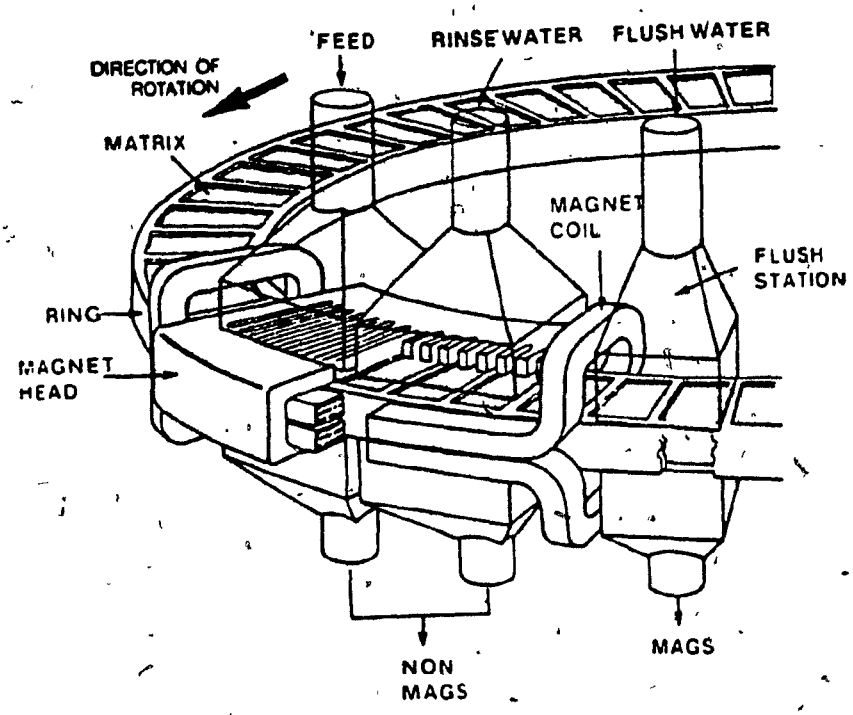

Figure 3 Continuous High Gradient Magnetic Separator.

magnetizing coil in HGMS is employed directly to magnetize the matrix. The working volume is the bore of the coil. In the HGMS design, the matrix serves only as a field gradient source and not as a flux conductor. Hence the volume occupied by the matrix can be smaller, usually 10-15%, compared to 60% in HIMS. This means that the HGMS can achieve a higher throughput for a given floor space. The matrix elements also can be made much smaller and the gradients correspondingly larger thus allowing fine and / or weakly magnetic particlesto be captured.

Unlike HIMS, the HGMS system controls the flow velocity through the matrix giving the field and the flowrate as operating variables (27). In principle no upper limit exists in the field avaliable for magnetizing the matrix., whereas in the HIMS the upper limit is when the iron electromagnet is saturated. This occurs at about 1.3Tesla. In a conventional solenoid the maximum field is at about 2Tesla.

Superconducting Separator: One of the drawbacks in large scale conventional HGMS is the high power consumption required to generate the magnetic field and the consequent need for cooling water. Superconducting devices can overcome the above problems. Some units are capable of producing 15Tesla over prolonged periods (28).

Figure 4 shows the principal features of a superconducting separator. It consists of a superconducting solenoid placed in a helium cryostat system necessary to

ERIEZ 50 KILOGAUSS SUPERCONDUCTING HIGH GRADIENT MAGNETIC SEPARATOR

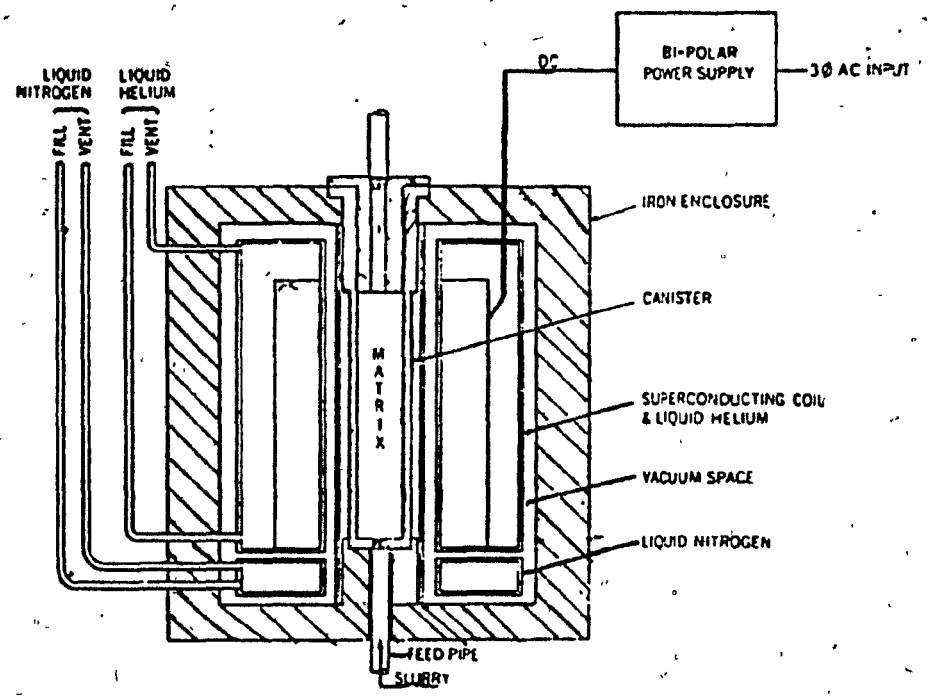

Figure 4 Superconducting Magnetic Separator.

retain liquid helium, otherwise the design is similar to conventional HGMS. There are altogether three cannisters, with matrices 0.5m long situated in the central bore. They can be moved by a hydraulic system (not shown) in a reciprociating mode so that while one matrix is in the magnetic field, the other is outside the field being cleaned by flushing. The reason for more than two matrices is to balance (minimise) the forces acting on the superconducting coil and also to reduce the force required to move the assembly back and forth.

1.2 BASIC PRINCIPLES OF MAGNETIC SEPARATION.

1.2.1 Magnetic Field of a Solenoid.

A solenoid is usually made with insulated copper wire wound on a tube of any electrical insulating material (such as plastic, fibre glass and rubber). A cross-section of a solenoid is shown in Figure 5. To derive a formula for magnetic flux density B at a point P on the axis of the solenoid due to current I flowing in the wires of the winding let:

L be the total length of the solenoid,

N be the total number of turns on the solenoid,

N/L is the number of turns per unit length,

r1 be the radius of the solenoid and

dx be the element of length of the solenoid.

Then there are (N/L)dx turns in the length dx and each turn contributes an element of magnetic flux density dB at P of

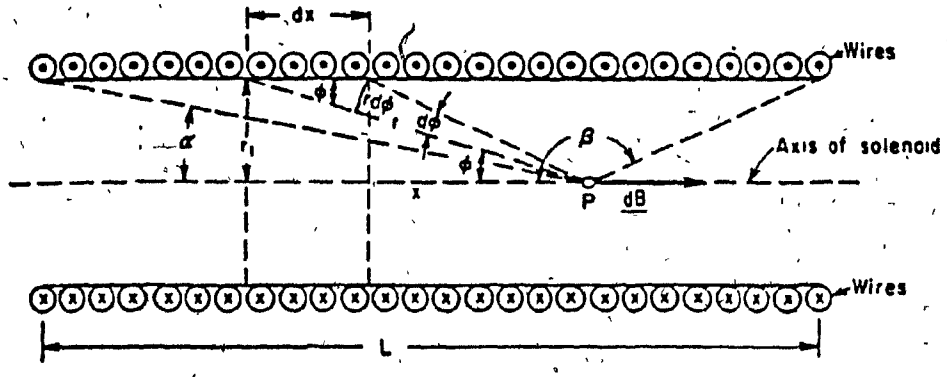

Figure 5 A cross-section of a solenoid.

the solenoid given by (30)

$$dB = (\mu_o I r1 (\text{Sin}\,\phi) N/2 r^2 L) \qquad \text{eq.(1).}$$

where ϕ is the angle between the axis and line drawn to dx from P.

d is thus the element of angle which subtends at P.

r is the distance from dx to P.

From the Figure $rd\phi$ = dxSin and $\text{Sin}\phi = r1/r$. Using these relationships to eliminate r, equation (1) becomes

$$dB = (\mu_o \frac{N\ I}{L}) \text{Sin}\,\phi\ d\phi \qquad \text{eq.(2).}$$

Hence upon intregating from α to β (Fig.5)

$$B = \mu \frac{N\ I}{2L} (\text{Cos}\ \alpha - \text{Cos}\ \beta) \qquad \text{eq.(3).}$$

where B is parallel to the axis of the solenoid. Equation 3 gives the magnetic flux density of the solenoid not only inside the solenoid but beyond the ends as well.

Where the length of solenoid is longer than its diameter D and P is not near either end, β is almost 180° and α is almost zero. Then equation 3 becomes

$$B = \mu_o \frac{N\ I}{L} \qquad \text{eq.(4).}$$

In this case the flux density is uniform across the area of cross-section of the solenoid, parallel to the axis of the

solenoid. At the end of the solenoid, $\beta = 90$ and α is almost equal to zero then

$$B = \mu_0 \frac{N I}{2L} \qquad \text{eq.(5).}$$

Comparison of equations 4 and 5 shows that the flux density on the axis at the end of a long solenoid has only half the magnitude as it has inside the solenoid. Figure 6 shows an approximate map of magnetic flux lines of a solenoid.

From the relationship between flux density B and field intensity H

$$B = \mu_0 H \qquad \text{eq.(6).}$$

it can be readily shown that by combining equations 6 and 4 that

$$H = \frac{N I}{L} \qquad \text{eq.(7).}$$

H is parallel to B. The units H are A/m and of B are T.

1.2.2 The Production of Alternating Magnetic Field.

From equation 7 it has been shown that the magnetic field intensity H, is directly proportional to the generating current I. For a solenoid connected to a sinusodial voltage source, the line voltage applied is given by Kirchoff's second law as following

$$v = Vm \sin \omega t = i Z_{magn} \qquad \text{eq.(8).}$$

where v is the instantaneous voltage,

Vm is the maximum voltage,

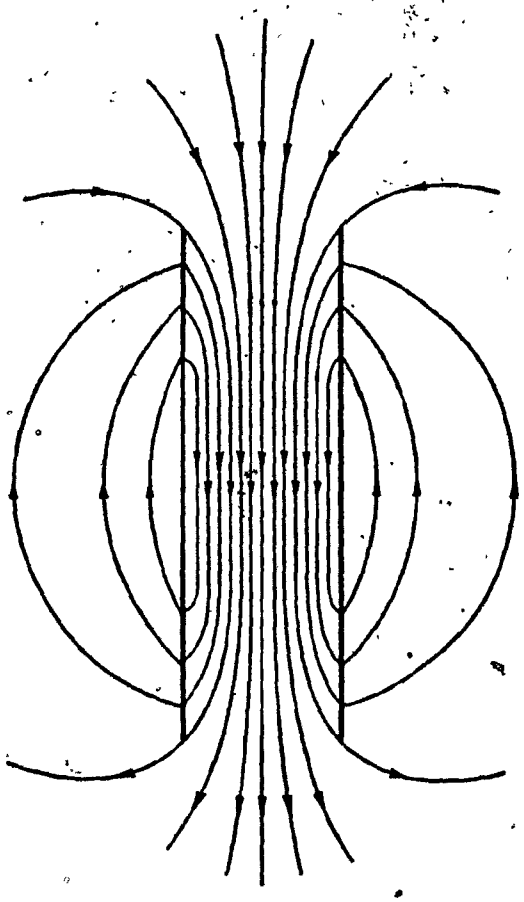

Figure 6 Magnetic flux lines of a solenoid.

w is the constant angular velocity,

t is the time,

i is the instantaneous current and

Zmagn is the magnitude of coil impedance.

By analogy with equation 8,

$$i = (Vm/Zmagn.) \sin wt \qquad \text{eq.(9).}$$

By Ohm's law

$$Im = (Vm/Zmagn.) \qquad \text{eq.(10).}$$

where Im is the magnitude of current from the source. Therefore equation 9 becomes

$$i = Im \sin wt \qquad \text{eq.(11).}$$

and on subtituting for i in equation 7, the magnetic field intensity H generated by a sinusodial voltage source is given by

$$H = (N/L)\, Im \sin wt \qquad \text{eq.(12).}$$

From equation 11 the current flowing in the solenoid is shown to be sinusodial. This type of current is called alternating current (a.c). Hence from equation 12 an alternating current will produce an alternating magnetic field intensity in the solenoid. Thus by analogy H can be expressed as follows

$$H = Hm \sin wt \qquad \text{eq.(13)}$$

where Hm is the magnitude of the magnetic field intensity in a solenoid at Im.

The field intensity produced by a direct current (d.c), corresponds to a constant value of Sin wt.

1.2.3 Competing Forces in High Gradient Magnetic Separators (HGMS).

In all magnetic separators there exists competion between magnetic and other forces (see Figure 7) (20). For magnetic and nonmagnetic particles the ratios of these forces are different. The magnetic force Fm, for a particle in a magnetic separator is given by the following expression

$$Fm = V\ Mp\ dB/dx \qquad \text{eq.(14).}$$

where V is the volume of the particle, m^3.

dB/dx is the field gradient, T/m

Mp is the magnetization of the particle, A/m.

The magnetization of a particle is a function of both the magnetic properties of the particle and the magnetic field to which it is subjected and it is expressed as follows

$$Mp = k\ H \qquad \text{eq.(15).}$$

where k is the particle suspectibility (dimensionless).

The value of k ranges from 10^{-5} to 10^{6} for very weak to very strong magnetic materials respectively. In some cases k assumes a negative value. Figure 8 shows the relationship between M and H for ferri and ferromagnetic materials; with increasing H, M rises rapidly and saturates. Figure 9 shows linear variation of M with H (21); a positive and negative slope are typical of paramagnetic and diamagnetic materials respectively.

Eq. 14 for magnetic force could be rewritten as

$$Fm = V\ k\ H\ \mu_o\ dH/dx \qquad \text{eq.(16).}$$

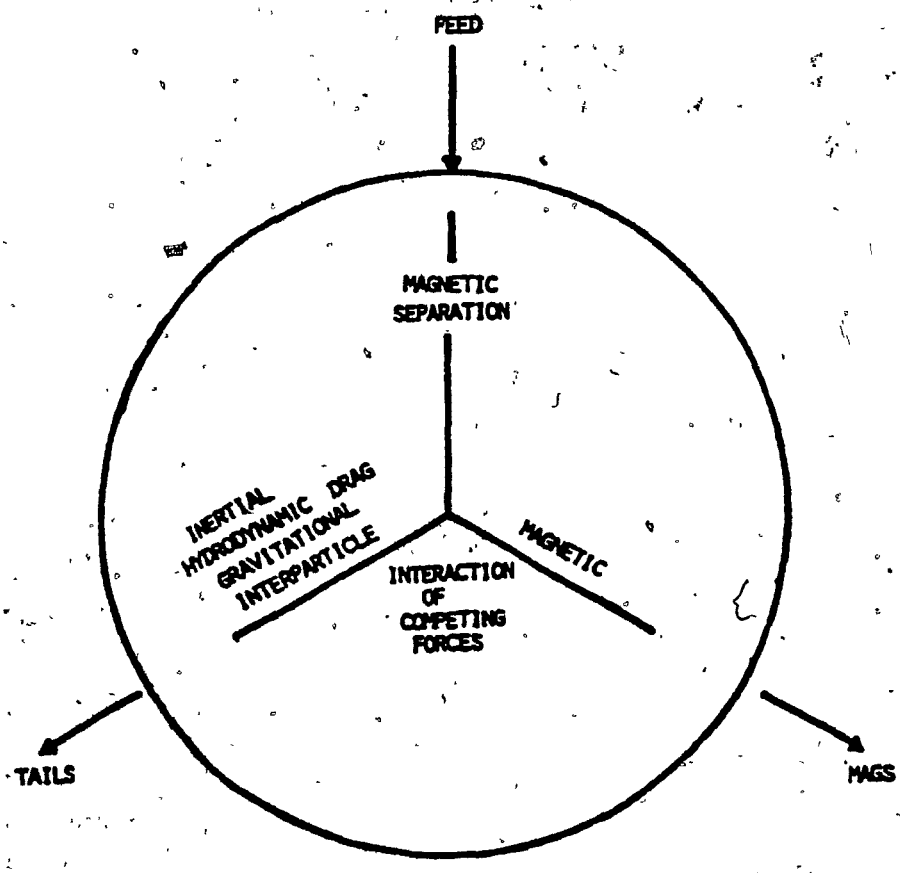

Figure 7 Competing forces in magnetic separation.

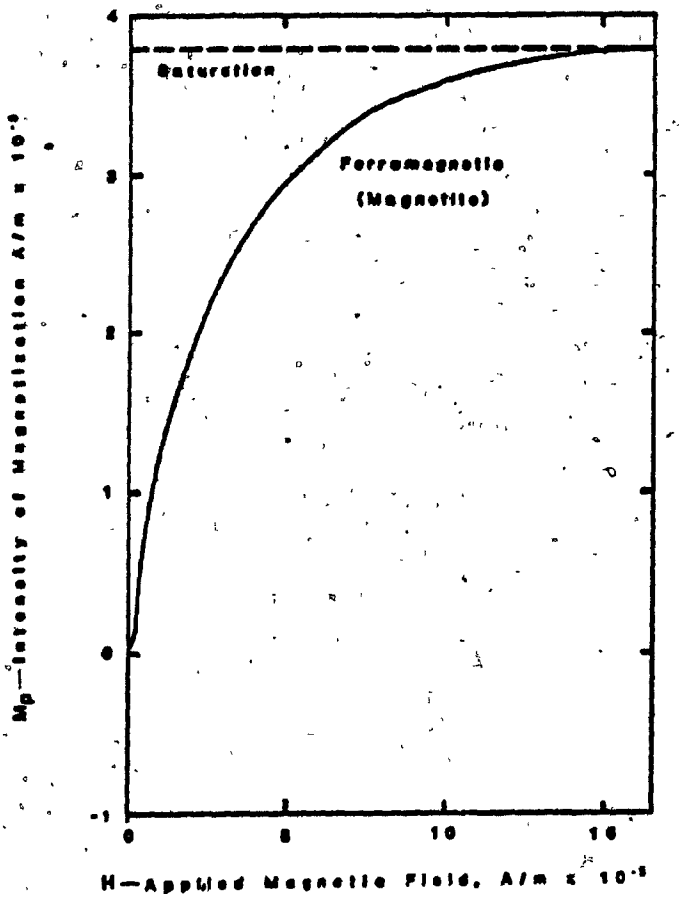

Figure 8 Relationship between magnetization,M, and field strength,H, for ferromagnetic material.

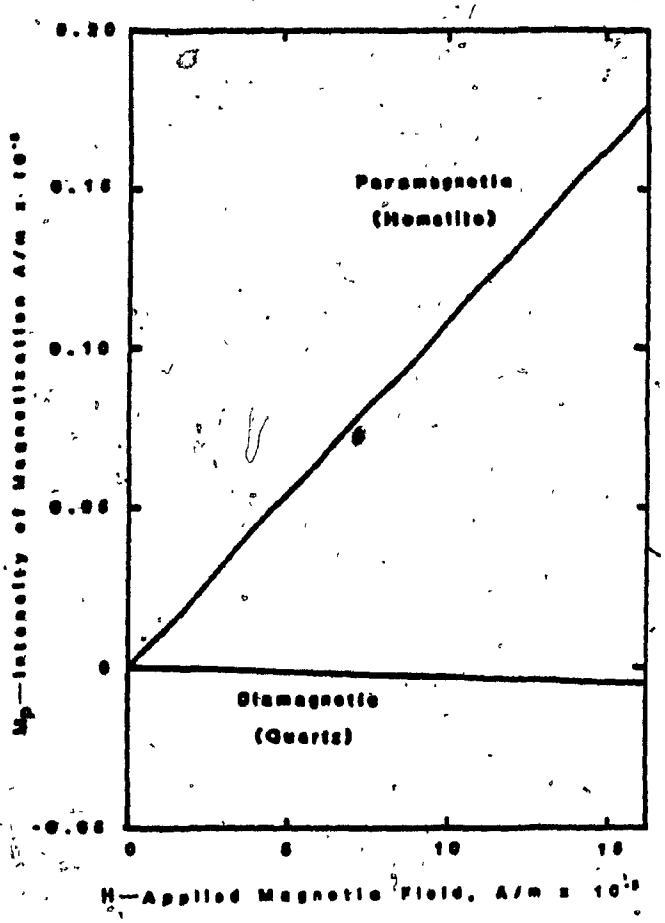

Figure 9 Relationship between magnetization, M, and field strength, H for para- and diamagnetic materials.

Thus the magnetic force for a particle in an a.c. solenoid magnetic separator would be

$$F_{a.c.} = V k H_m \sin \omega t \, \mu_0 \, dH/dx \qquad \text{eq.(17).}$$

$$dH/dx = \sin \omega t \, d/dx + \sin \omega t \, dH_m/dx.$$

Therefore

$$F_{a.c} = V k \mu_0 H_m ((\sin^2 \omega t \, dH_m/dx) + (\sin^2 \omega t \, d/dx)) \qquad \text{eq.(18).}$$

since Sin ωt is not a function of x, the last term of eq.18 equals zero. Hence

$$F_{a.c.} = V k H_m \mu_0 \sin^2 \omega t \, dH_m/dx \qquad \text{eq.(19).}$$

From equation 19, the force on a particle in an a.c. magnet will always be positive since $\sin^2 \omega t$ is greater than zero.

The major competing force against the magnetic force in a wet system is the hydrodynamic drag force. Assuming for a spherical particle with a Stokesian flow regime, the hydrodynamic drag force is given by

$$F_d = 6 \pi b v \eta \qquad \text{eq.(20).}$$

where b is the particle radius, m.

v is the relative velocity of the particle to the fluid (water). m/s. and

η is the fluid viscosity, kg/m/s.

1.3 MAGNETIC FLOCCULATION.

The phenomenon of flocculation (or aggegation) of ferromagnetic particles in a magnetic field has been described by Lomovtsev et al (31). They distinguished three phases. First, when the particles are in a relatively weak

field they become magnetized and align themselves with the line of force. The second phase occurs in a stronger field, where the individual grains act as secondary magnets. Now the grains begin to gather into groups and flocculation occurs. Depending on the nature of the field and the propeties of the mineral, the flocs adopt various forms, e.g. they may become long chains or aggregates resembling half an ellipsoid of rotation. The tips of the flocs point towards the poles of the field. When the magnetic force acting on the flocs exceeds the sum of the forces opposing it, the third phase begins: the floc attaches to the surface of the magnet or magnetizing body; in the case of hgms this is the matrix.

1.3.1 Theory of Magnetic Flocculation.

Several theories of magnetic flocculation have been postulated. Among them is the work of Eyssa and Boom (32). They developed a theory for the flocculation mechanism by studying the coagulation or flocculation force between magnetic particles in a suspension brought into a magnetic field. The flocculation force will depend on the particle magnetization and the suspension porosity. The slurry was treated as an infinite slab of thickness 2L, see Figure 10, where

$$L = N r \qquad \text{eq.(21).}$$

N is the number of particles along the length L;

r is the interparticle distance,

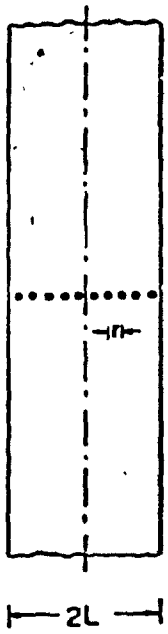

Figure 10 The interparticle distance, r, in an infinite slurry slab of thickness 2L.

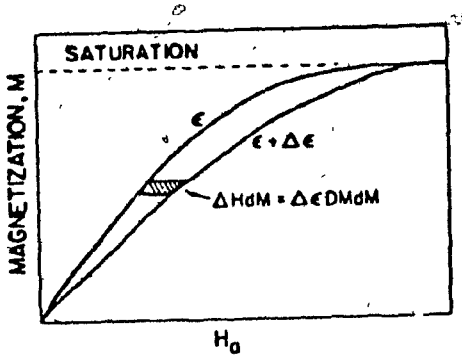

Figure 11 The change in energy stored per particle due to porosity change.

$$r_1 = \frac{b}{(3/4\pi(1-e))^{1/3}} \qquad \text{eq.(22).}$$

where b is the particle radius,

e is the porosity of the suspension, and

(1-e) is the solids fraction of the slurry.

Since the attraction force between two dipoles is proportional to r^{-4} only the effect of the nearest particles are considered. This means that the particles on a surface have a high attraction force towards the interior while other particles have much smaller net forces on them. Hence only the effect of the forces on the particles in contact with the surface are considered.

By allowing the slab to shrink and change its porosity from e to e+de then the flocculation force F can be estimated from change in energy stored dE from the relation

$$dE = F\, dL \qquad \text{eq.(23).}$$

where dL is the distance the particle moves.

$$dL = N\, dr$$

$$= \frac{N\,(4/3\,\pi)^{1/3} b\, de}{3\,(1-e)^{4/3}} \qquad \text{eq.(24).}$$

The energy E taken from the particle during a porosity change e to e+de as shown in Figure 11; it is the area between the two curves multiplied by the particle volume.

$$\delta E = V \int dH\, dM \qquad \text{eq.(25),}$$

where δE is the energy stored per particle,

$$dH = de\ D\ M \qquad \text{eq.(26).}$$

D is the demagnetizing factor of the slurry.

then

$$\delta E = \upsilon \int_0^M de\ D\ M\ dM \qquad \text{eq.(27).}$$

$$= 1/2\ de\ D\ M^2\ (4/3\pi)\ b^3 \qquad \text{eq.(28).}$$

The total energy change dE in a column of N particle is given by

$$dE = N\delta E \qquad \text{eq.(29).}$$

Combining eqs. 24 and 29 gives

$$F = 3.898\ D\ M^2 b^2\ (1-e)^{4/3} \qquad \text{eq.(30).}$$

This attractive force divided by the gravitational force, assuming a spherical particle for which D = 4π/3 is:

$$F/mg = 3.898\ M^2\ (1-e)^{4/3}/pg\ b \qquad \text{eq.(31).}$$

where p is the particle density, and

g is the gravitational acceleration.

Figure 12 shows F/mg as a function of (1-e) for different sizes of saturated magnetite particles. One consequence is that calculation of the force on a highly magnetic particle should take into account the nearby particles.

1.3.2 Demagnetizing of Ferromagnetic Material.

When particles of ferromagnetic material have been removed from a magnetic field, residual magnetism causes

flocculation. For depolarization or elimination of this

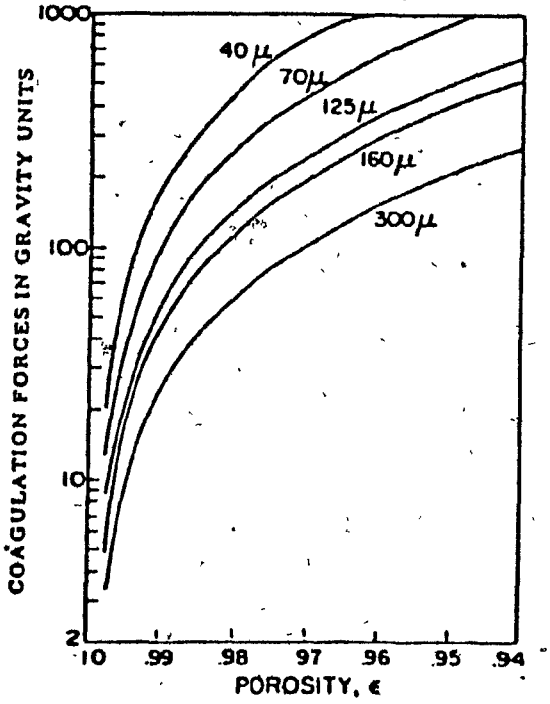

Figure 12 Coagulation forces versus porosity on saturated magnetite particles.

residual magnetism alternating coils have long been used because they represent the most pratical of the two available methods for performing depolarization (the other method being that of heating the material to the Curie point and then cooling it under zero field conditions (33-35)). Depolarizing can be considered magnetic deflocculation. The terms demagnetizing and randomizing are also used.

In the literature there appears to be a lack of information on the subject of demagnetization. Although Dean and Davis (35) touch on this problem in their work most of the data are quite qualitative in nature. In 1918 E. W. Davis was granted a patent for demagnetization of magnetite pulps (36). His method involved passing the pulp through a tappered coil activated by an alternating current of normal frequency 60Hz. This method, with minor modifications has been used almost universally in installations where depolarization of low coercive force materials has been required.

Hartig, Onstad and Foot (35) made a detailed study of the factors involved in depolarizing both low (below 100 Oe) and high (above 100 Oe) coercive force material. They developed a method of evaluating the relative degree of demagnetization of any pulp based on the settling characteristics of the pulp. With flowing pulps, they found that depolarizing was less complete than in the static state, but this effect could be overcome by increasing the field strength, for example, from 500 to 700 Oe rms (root

mean square or effective value). Using magnetite only, Williams and Hendrickson, (37). in their work substanstiated the findings of Hartig et al, that slow withdrawal from a.c. field of 550 Oe or more was equivalent to depolarizing by the Curie treatment.

In classification of pulps containing magnetized ferromagnetic particles, demagnetization is of great importance. An example is in the first benefication of magnetic taconite ore, where demagnetization made the use of a closed grinding circuit possible. The product from the mill was also demagnetized before gravity concentration(35).

In coal washery plants the magnetic media used in the sink - float process are magnetite and ferrosilicon. To reduce medium viscosity, the medium is dispersed using demagnetizing coils.

Heikki (34), working with titaniferous magnetite, reported that demagnetization markedly enhanced the separation of silicates and ilmenite.

In studying the behaviour of magnetic particles under a microscope, Hartig et al (35) observed that in a 60Hz field single particles rotated presumably at a speed of 60rps, in much the same fashion as the rotor of a synchronous electric motor. He also observed that if a group of particles were placed in close proximity in an alternating field of gradually increasing intensity the particles would at first rotate and then tend to form into groups, or chains. These chains are formed as a result of

mutual forces of attraction between particles due to the field induced in each particle by the applied field. After the chains form the forces of attraction holding them together were large enough to prevent rotation.

The chaining of particles appears to be of considerable importance in the demgnetization process in a medium of low viscosity such as water. The chaining effect of ferromagnetic particles is considered to be why good demagnetization is not achieved (34).

The study undertaken in this thesis is different in that demagnetization was not just done before separation, but separation was done in the demagnetization (a - c) field.

1.4 MODEL OF GRADE OF MAGNETIC PRODUCT

1.4.1 Obertueffer Model

Obertueffer, (20) postulated a model for recovery, Rm and grade, Gm of magnetic product. By considering the effect of interaction between magnetic force, Fm, and competing forces, Fc, in a magnetic separation. Obertueffer used a simple propability approach and defined

$$Gm = \frac{Rm}{Rm + A\ Rnm} \qquad \text{eq.(32).}$$

where Rnm is the recovery of nonmagnetic particles in magnetic product, A is the mass ratio of the nonmagnetic to the magnetic particles in the feed. Assuming

$$Rnm = K' Rm \frac{Fi}{Fc} \qquad \text{eq.(33).}$$

where K' is a proportionality constant and Fi/Fc is the ratio of interparticle to competing forces (constant ratio in this case).

Then equation (33) becomes

$$Gm = \frac{1}{1 + A K} \qquad \text{eq.(34).}$$

where K = K' (Fi/Fc).

Linearizing eq.(34), we have

$$\frac{1}{Gm} = 1 + A K \qquad \text{eq.(35).}$$

A plot of 1/Gm versus A should yield a straight line with slope of K.

1.4.2 'Void-Filling' Model

In this model, filling of the voids in the magnetite is considered.

Let Uv be the volume fraction of voids in the absence of nonmagnetics (for example silica)

fv be the fraction of Uv filled by silica

Assume, maximum fv = Uv

therefore

mass of magnetite = $(1 - Uv)\ Pm$ eq.(36).

and mass of silica = $fv\ Uv\ Ps$ eq.(37).

where Pm is the density of magnetite (magnetic particle).

Ps is the density of silica (nonmagnetic particle).

then the grade of magnetic product is defined as

$$Gm = \frac{(1 - Uv)\ Pm}{(1 - Uv)\ Pm + fv\ Uv\ Ps} \qquad \text{eq.(38).}$$

or the minimum grade, Gm

$$Gm = \frac{(1 - Uv)\ Pm}{(1 - Uv)\ Pm + Uv^2\ Ps)} \qquad \text{eq.(39).}$$

For a given particle size, assume fv can be related to A by

$$fv = Uv\ (1 - \exp(-aA)) \qquad \text{eq.(40).}$$

where a is the "probability of silica retention per unit of A".

Substituting eq.(40) in eq.(38), therefore

$$Gm = \frac{(1 - Uv)\ Pm}{(1 - Uv)\ Pm + Uv^2\ Ps\ (1 - \exp(-aA))} \qquad \text{eq.(41).}$$

Linearizing eq.(41)

$$\frac{1}{Gm} = 1 + \frac{Uv^2\ Ps\ (1 - \exp(-aA))}{(1 - Uv)\ Pm} \qquad \text{eq.(42).}$$

As A approaches infinity, exp(-aA) equals zero; therefore

$$\frac{1}{Gm} = 1 + \frac{Uv^2\ Ps}{(1 - Uv)\ Pm} \qquad \text{eq.(43).}$$

This permits Uv to be estimated from the measured minimum grade. By re-arranging

$$-aA = \ln\left(1 - \frac{Pm\ (1 - Uv)}{Ps\ Uv^2}\ (1/Gm - 1)\right) \qquad \text{eq.(44).}$$

The plot of this ln function versus A should give a straight line with slope a.

2. EXPERIMENTAL WORK

2.1 APPARATUS.

2.1.1 Description of High Gradient Magnetic Separators.

The separators used for the experiments were laboratory batch sparators, an a-c powered solenoid magnet, and a d-c powered solenoid magnet.

The a-c hgms: This was an Eriez demagnetizing solenoid type-2DR. It operated on a 550volt, 60cycles single phase alternating current power source. Figure 13 shows the dimension of the coil. The solenoid consisted of copper wire wound around a spherical plastic core such that the magnetic field in the core increases uniformally from one end of the coil to peak at its centre. The current intake was 1.45 A(rms) and wire resistance was 32 ohms (rms). Thus the power or energy loss, $I^2 R$ was sufficiently low that cooling was not required during operation. From these coil specifications, the magnetic flux intensity generated was 600 +/- 10 Gauss or 0.06Tesla(rms). Usually for solenoids capable of fields larger than about 1000 Gauss or 0.1Tesla(rms) cooling of the winding becomes necessary.

The demagnetizing solenoid was mounted on a wooden board at a minimum of 10cm from the nearest metallic object and arranged so that plexiglass tubing for slurry transportation passed vertically through the coil core. The electrical connection to the solenoid was through a junction box mounted on one end of the coil. The junction box has a

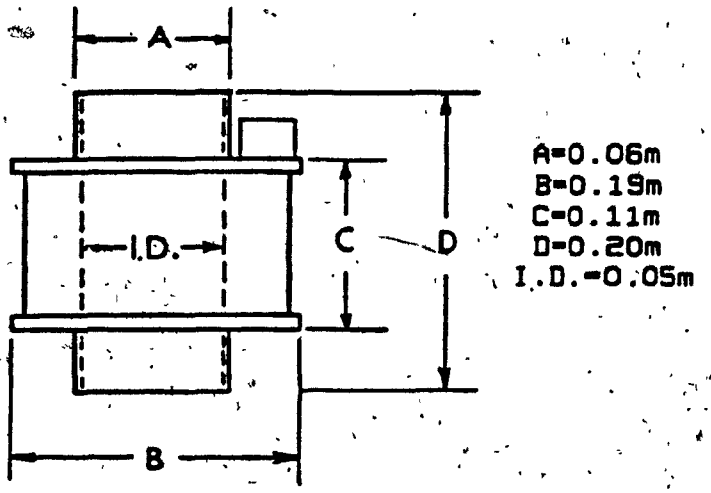

Figure 13 Eriez demagnetizing solenoid type-2DR.

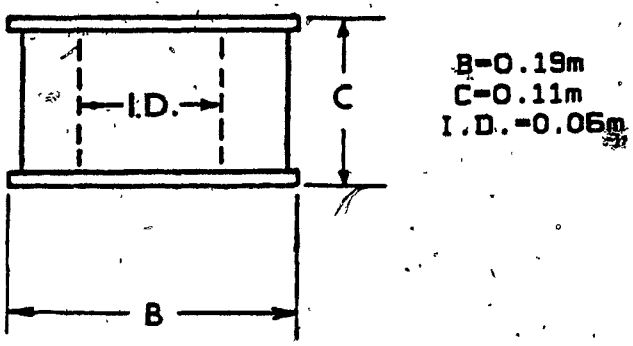

Figure 13a The electromagnetic coil.

standard size conduit to which a wire from the coil connected the wire going to the voltage alternating current source. Hence the maximum magnetic field generated in the core of the coil was directly proportional to the maximum alternating current of the coil.

The d-c hgms: The electromagnetic coil used was taken from a Davis tube separator. Its iron core was removed to create an opening in which plexiglass tubing for slurry transportation was passed. Figure 13a shows the solenoid dimensions. The coil was operated from a 110VAC power source. Figure 14 shows the solenoid electrical circuitry. The generation of magnetic field in the solenoid was through the alternating current voltage passed into a 120volts a.c. variac and rectified into a d.c. voltage. The variac was set to give a direct current flow into the coil to give an equivalent magnetic flux intensity as in the demagnetizing solenoid. The current was monitored on a multimeter connected to the rectifier.

2.1.2 The Difference Between A.C. and D.C. Solenoids:

This is due to their impedance (Z) expressed as

$$Zcoil = Rcoil + jXcoil \quad ohm \qquad eq.(45).$$

where Rcoil is the coil wire resistance

jXcoil is the magnitude of imaginary part of the impedance, which is a function of Frequency (f)

j is the imaginary number $\sqrt{-1}$.

Xcoil is coil reactance, $X = wLc = 2\pi fLc$

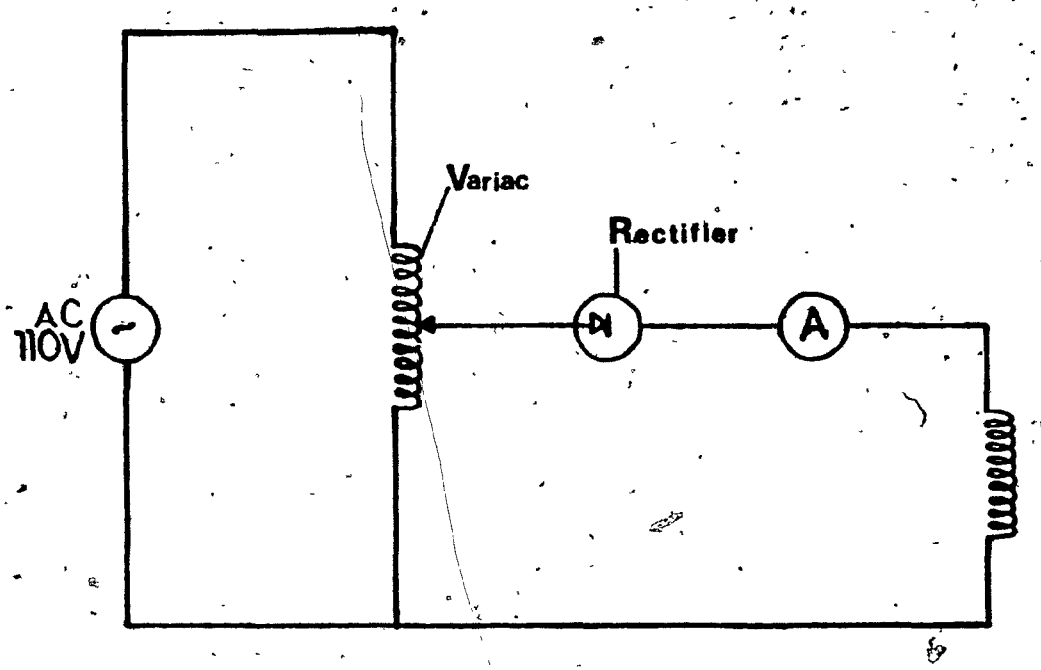

Figure 14 Direct current coil electrical circuitry.

Lc is the inductance, an intrinsic property of coil (approx. constant).

The frequency of excitation in a d.c. solenoid is equal to zero, therefore Z = R in eq.(45). Hence an a.c. solenoid will have more impedance due to reactance than a d.c. solenoid. As a result the a.c. solenoid will require higher voltage for the same magnitude of magnetic field intensity compared with the d.c. solenoid.

2.1.3 The Effect of Type of Current Generating Field in a Solenoid:

This is illustrated by Ohm's law given as

$$I = V/Z \qquad \text{eq.(46).}$$

and rewritten as

$$V = Z\,I \qquad \text{eq.(47).}$$

analogically

$$V_{a.c.} = Z\,I_{a.c.} \qquad \text{eq.(48).}$$

$$V_{d.c.} = Z\,I_{d.c.} \qquad \text{eq.(49).}$$

The current I is known to be a function of the voltage. Hence to generate the same magnitude of magnetic field intensity for a given solenoid, less Id.c. than Ia.c. would be required and also a lower Vd.c..

2.1.4 Matrix and Sample Transporting Sytem.

Two types of expanded wire matrices were used for the experiments. Figure 15 shows the matrices. Matrix A

Lc is the inductance, an intrinsic property of coil (approx. constant).

The frequency of excitation in a d.c. solenoid is equal to zero, therefore Z = R in eq.(45). Hence an a.c. solenoid will have more impedance due to reactance than a d.c. solenoid. As a result the a.c. solenoid will require higher voltage for the same magnitude of magnetic field intensity compared with the d.c. solenoid.

2.1.3 The Effect of Type of Current Generating Field in a Solenoid:

This is illustrated by Ohm's law given as

$$I = V/Z \qquad \text{eq.(46).}$$

and rewritten as

$$V = Z\,I \qquad \text{eq.(47).}$$

analogically

$$V_{a.c.} = Z\,I_{a.c.} \qquad \text{eq.(48).}$$

$$V_{d.c.} = Z\,I_{d.c.} \qquad \text{eq.(49).}$$

The current I is known to be a function of the voltage. Hence to generate the same magnitude of magnetic field intensity for a given solenoid, less Id.c. than Ia.c. would be required and also a lower Vd.c..

2.1.4 Matrix and Sample Transporting Sytem.

Two types of expanded wire matrices were used for the experiments. Figure 15 shows the matrices. Matrix A

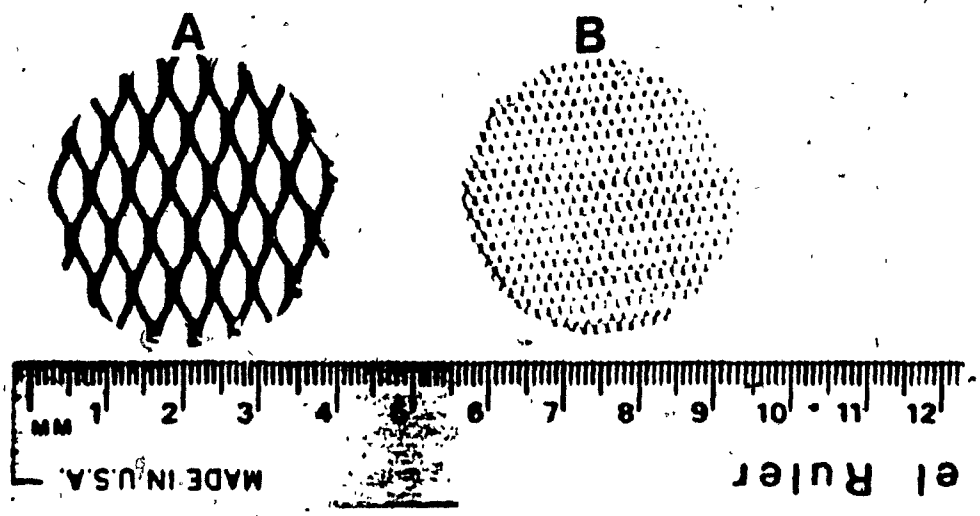

Figure 15 The ferromagnetic matrix A (regular) and B (fine).

(regular/coarse matrix) contained 13 pieces of expanded metal mesh with a disc diameter of 3.8cm and holes diameter of 3.8mm. Matrix B (fine matrix) contained 21 pieces of expanded metal mesh with a disc diameter of 3.8cm and holes diameter of 1 mm. Both matrices weighed 30gm. Each were prepared by packing upon each another at right angles and were held in cannisters 10cm long by 3.8cm I.D. and 10cm by 4.3cm O.D. plexiglass cannisters respectively. The cannisters were connected at both ends to 15cm long plexiglass tubing with a 4.5cm I.D. plexiglass adaptor. At the bottom end, the plexiglass tube was connected to a copper tube 35cm long by 1.3cm diameter. At the top end copper tubing 60cm long by 1.3cm diameter with expanded ends of 4.9cm I.D. connected the plexiglass tubing to a water tank of 2.75Litres.

A feed tank with a plastic stirrer connected to an electric motor was suspensed over the water tank. Tygon tubing with an off/on valve connected the feed tank through the water tank into the copper tubing. Slurried sample was gravity fed via the plastic tube from the feed tank through the separating zone and into a collecting bucket. Figure 16 is a schematic diagram of the sample transport system.

All tests were run using a constant head of 72cm from the bottom of the head tank to the centre of the matrix. Two ball valves were placed at 30cm and 37cm above the cannister on line in the copper tube to act as on/off valves. Another on/off valve was at 40cm below the cannister

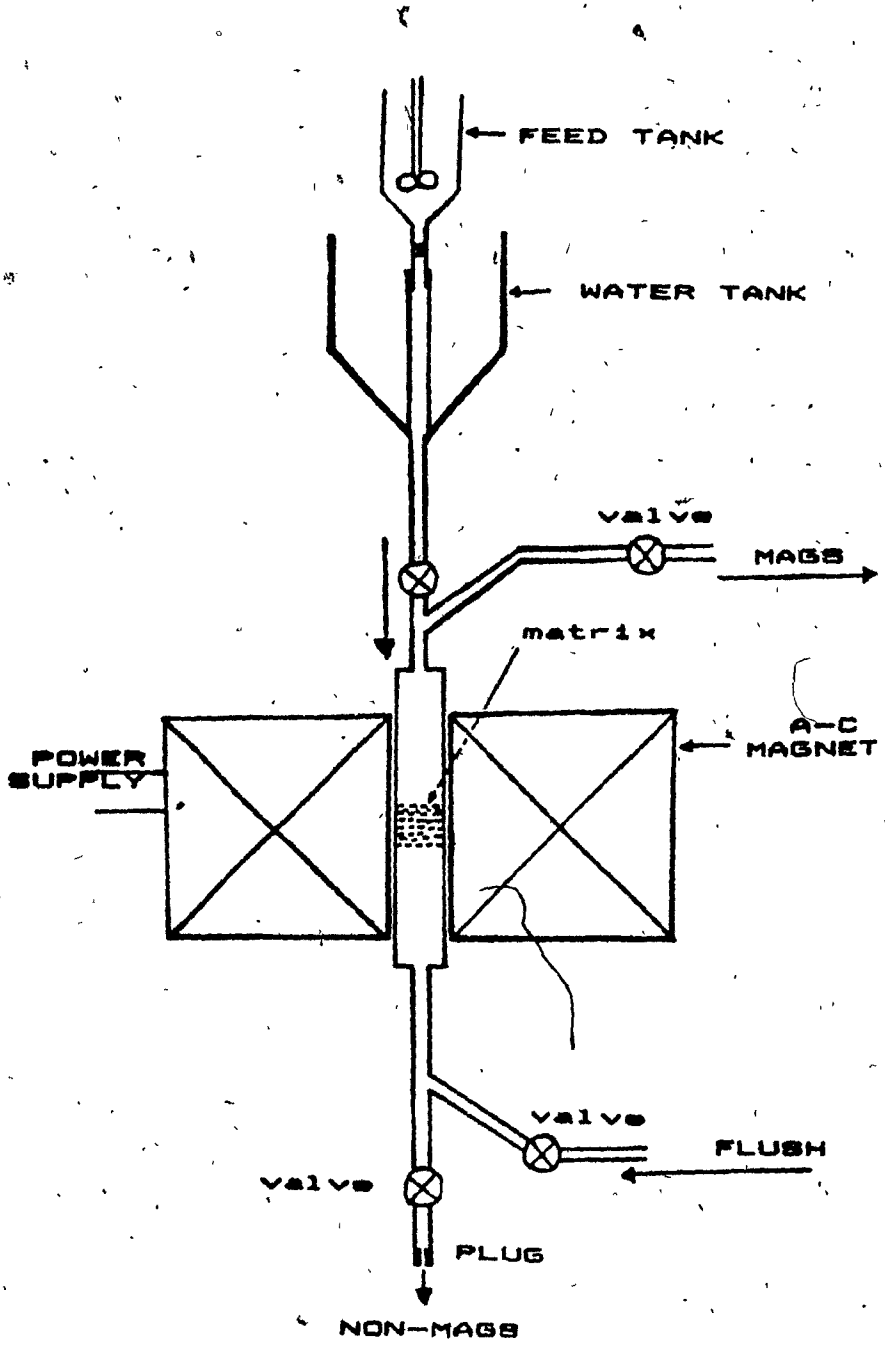

Figure 16 Schematic diagram of sample transport system.

while 1.3cm Tygon tubing with a set of bored, brass plugs placed in line to control flow rate was attached 10cm below the valve. Each plug had a different I.D. to give a range in flow velocity through the cannister matrix. This way reproducible velocities are reliably attained. The total head from the bottom of the head tank to the brass plug was 1.10m.

2.1.5 Calibration of the Solenoids.

In chapter 1, it was demonstrated that the magnetic field strength in the core of a solenoid is directly proportional to the electric current flowing through it. To calibrate the magnetic field strength produced in the cores of the demagnetizing and electromagnetic solenoids, the Hall effect method was used (Figure 17). This was done first by pre-calibrating a Hall effect crystal probe model HR-66 in a known variable field strength electromagnet with a gaussmetre. The relationship between the millivolt output of the Hall probe and the gaussmetre readings is plotted in Figure 18.

Both solenoids separately were then calibrated using the Hall probe crystal by suspending it at the centre of the solenoid core, and recording the millivolt output at set current inputs from the magnet power supply. These millivolt readings were converted to field strength values using Figure 18. The linear relationship between the solenoid field strength and direct current input in the solenoid is

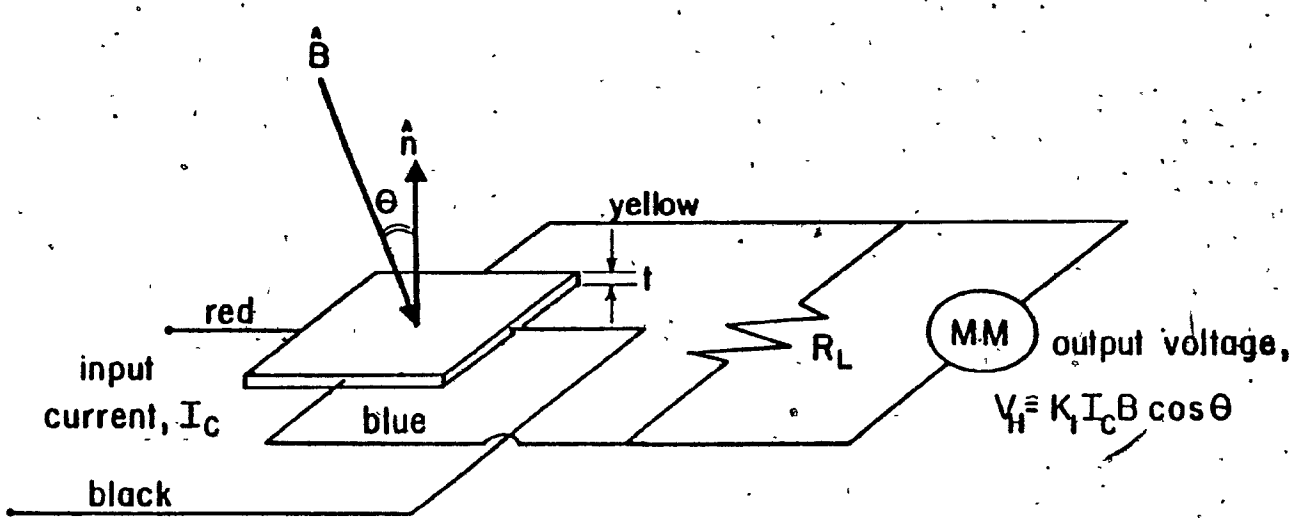

Figure 17 The hall effect probe set up.

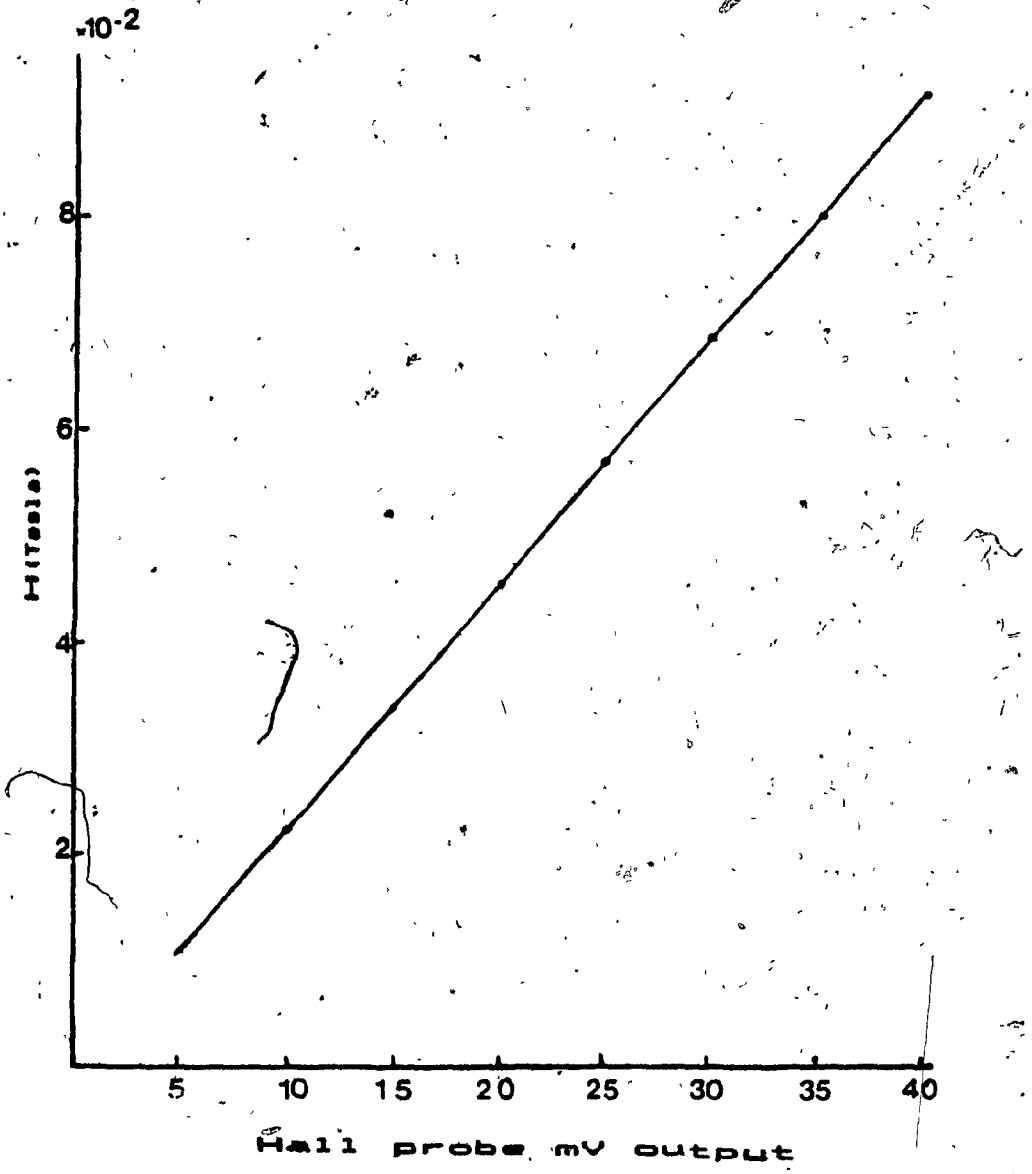

Figure 18 Calibration of hall probe mV output to field strength, H.

shown in Figures 19 and 20 for the a.c. demagnetizing coil and d.c. electromagnet coil respectively.

The a.c. solenoid magnetic field is expressed by:

$$Ha.c. = 3.294\ I\ 10^{-2} - 1\ 10^{-4} \qquad \text{eq.(50).}$$

and for d.c. solenoid magnetic field is given by:

$$Hd.c. = 8.79\ I\ 10^{-2} + 7\ 10^{-4} \qquad \text{eq.(51).}$$

The difference in H is due to the N/L which are properties of the solenoid.

The Hall crystal was also used to determine the profile of field strength along the axis of the two solenoids. The plots of the field strength profile are shown in Figures 21 and 22. It was observed that the field strength along the solenoid axis increases gradually with distance from one end and reached its peak or maximum at the centre. Also within 2cm on both sides of the axis centre, the field strength was found to be uniform. This allowed a 4cm working space within which to place the matrix to exploit a uniform field.

2.1.6 Mechanical Vibration.

For the purpose of investigating the effect of vibration on magnetic separation, a mechanical vibrator taken from a Frantz isodynamic magnetic separator was coupled to the upper end, where the plexiglass tubing with the regular matrix cannister and the copper tubing were connected.

The vibrator was plugged directly into a 110VA.C.

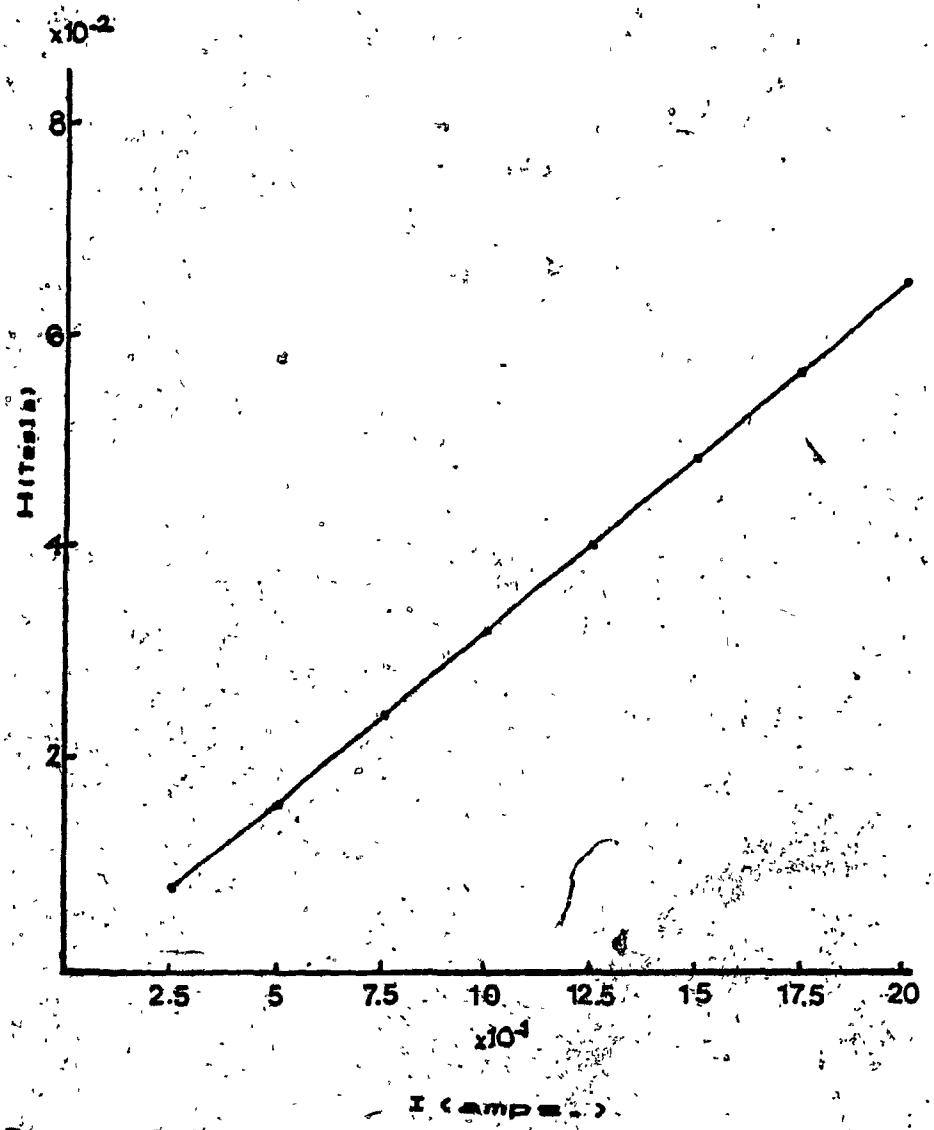

Figure 19 Calibration of the a.c. demagnetizing solenoid field strength supply by the generating current.

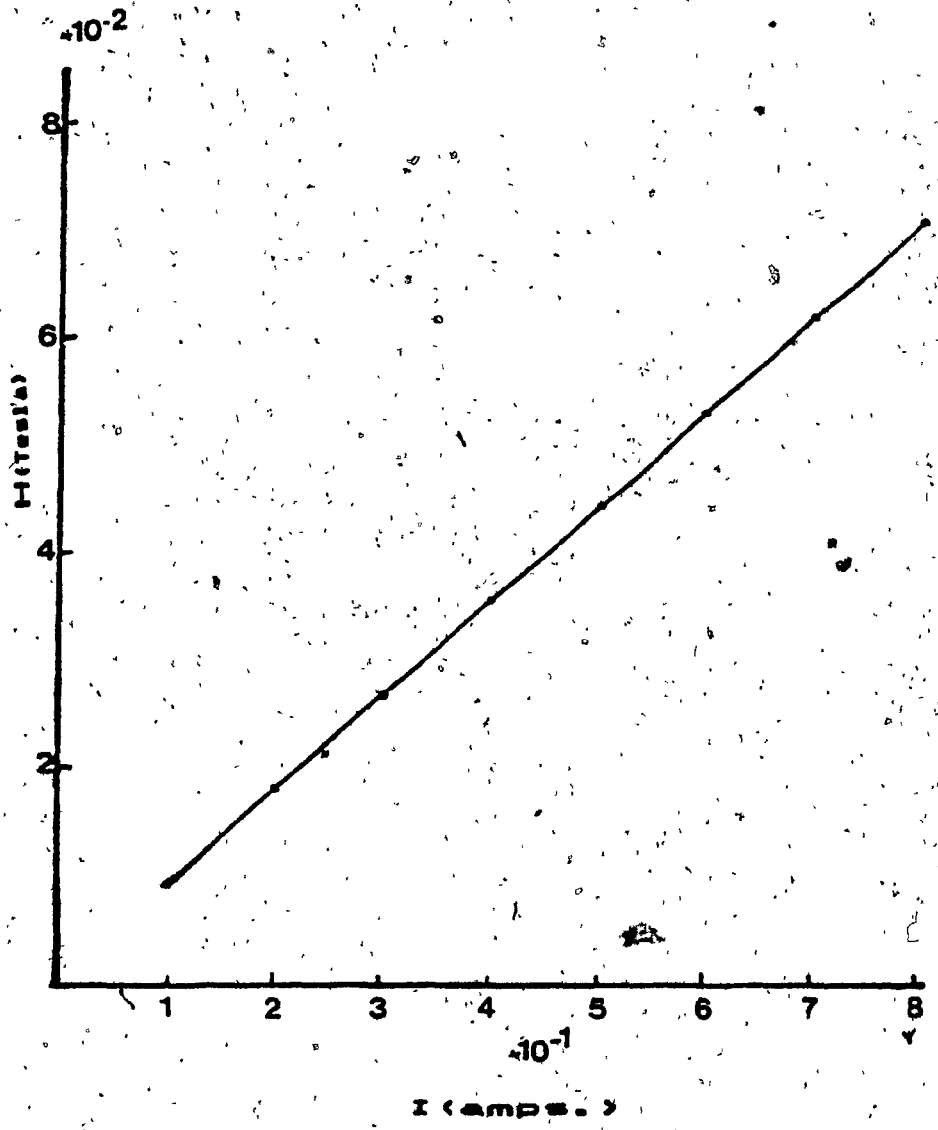

Figure 20 Calibration of the d.c. electromagnetic coil field strength supply by the generating current.

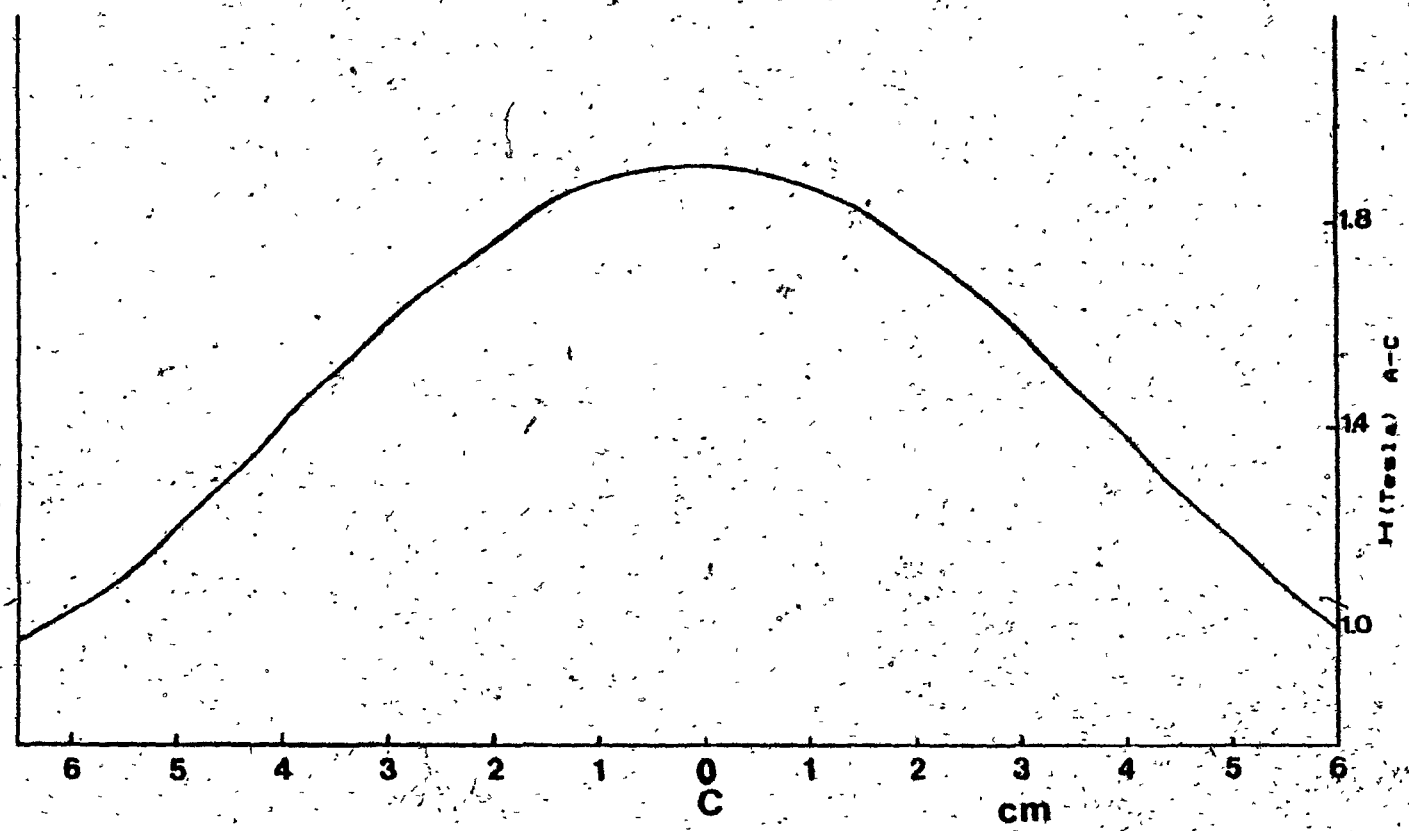

Figure 21 Field strentgh profile in the a.c. solenoid.

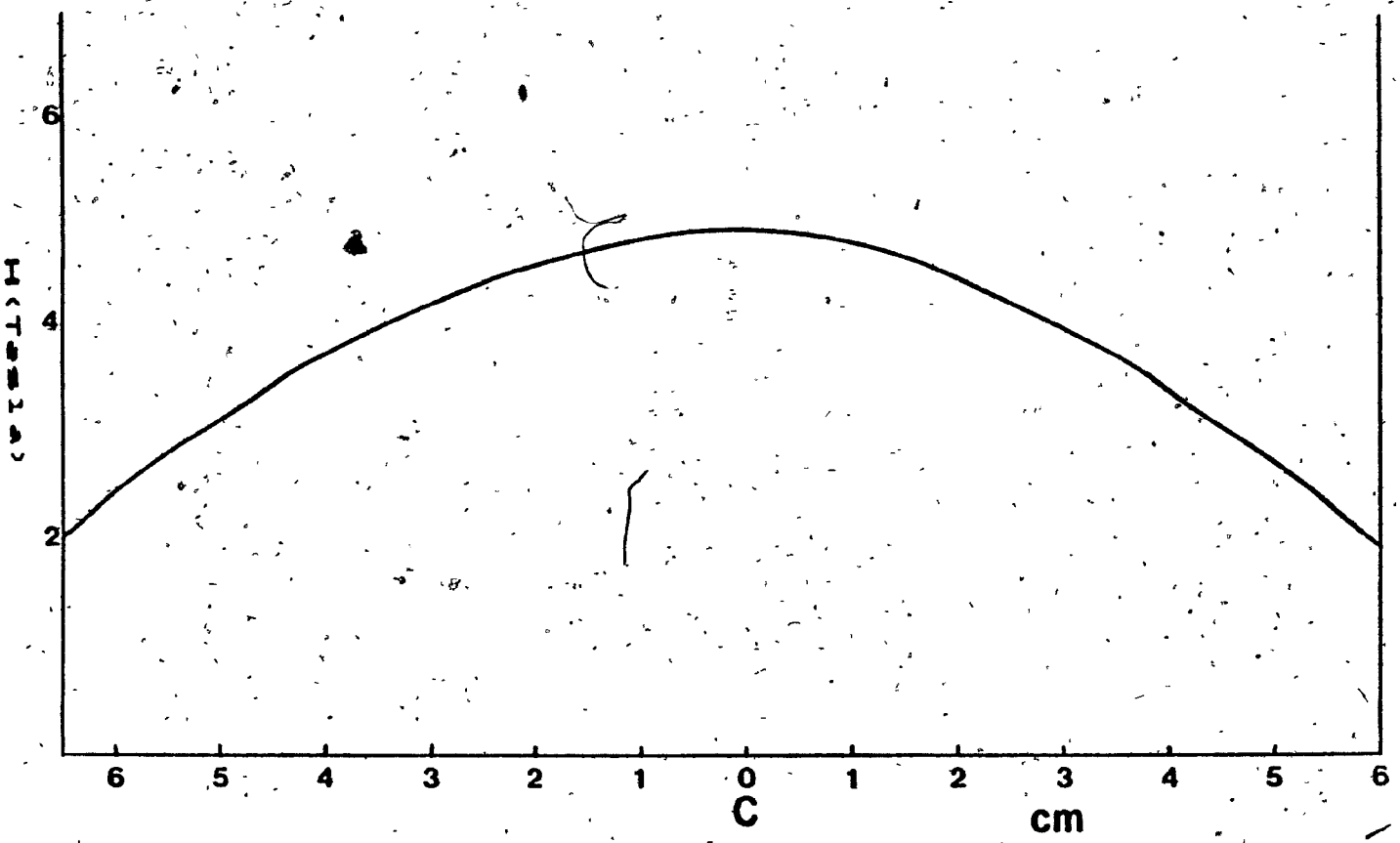

Figure 22 Field strength profile in the d.c. coil.

source and vibration was measured using a precalibrated accelerometer afixed to a known mass of regular matrix in the cannister. Calibration was done with the vibrator off and on for background and actual measurements in the d.c. magnet (Table 1). The same instrument was used for the a.c. magnet. Introduction of water showed no significant change in vibration.

2.2 SAMPLE PREPARATION.

Three pure mineral samples, magnetite, silica and barytes were prepared for use in the experiments for separation on the HGMS. All the mineral samples were screened through a 400mesh sieve placed on a wet vibrating sieve shaker "Analysette 3". The minus 400mesh fraction was further sized using the Warman Cyclosizer into 5 cone fractions according to the mineral particle's settling velocity. For magnetite, silica and barytes the particle sizes for each cone are given in Table 2. The operation of Warman Cyclosizer has been described in detail by Kelsall and McAdam(38).

2.2.1 Pure Magnetite.

5gm of pure magnetite of cones 2, 3, 4, 5, and -5 respectively were prepared and passed through the two separators to ensure that all the magnetite was captured under the selected conditions (that is, recovery in each case is 100%).

TABLE 1

MECHANICAL VIBRATOR MEASUREMENT WITH AN ACCELEROMETER (BRUEL & KJAER, TYPE4339)

ACCELERATION (m/s^2)	VELOCITY (m/s)	DISPLACEMENT (m)
BACKGROUND		
0.045	0.0001	0.00006
VIBRATOR ON		
35	0.05	0.00005
PLUS WATER		
33	0.06	0.00005
VIBRATION IN A. C. HGMS		
0.2	0.002	0.00005

TABLE 2

PARICLE SIZE

OF MINERALS IN WARMAN CYCLOSIZER.

CONE NUMBER	AVERAGE PARTICLE SIZE (μm)		
	MAGNETITE	SILICA	BARYTES
1	28.44	47.87	32.94
2	21.63	36.41	25.06
3	16.12	27.13	18.67
4	11.1	18.69	12.86
5	8.67	14.59	10.04

2.2.2 Mixture Samples

a) Equal Cone Mixtures of Magnetite and Silica.

5gm of magnetite was mixed with silica to give mass ratios from 1 to 6 for every individual cone size 2, 3, 4, and 5. The silica to magnetite mass ratio for cone 2 was extended to 10. This ensured mixtures were of particles having equal settling velocities so that both magnetite and silica arrived at the magnetized matrix at the same time.

b) Equal Cone Mixtures of Magnetite and Barytes.

Mixtures of cones 2 and 5 at mass ratios 1 and 6 were used. Barytes was used to give a mineral with similar density to the magnetite and thus a closer size than that obtained between magnetite and silica.

c) Samples for Mechanical Vibration.

5gm of magnetite was mixed with silica at mass ratio 1 to 6 for cone 2 only.

d) Mixed Cone Sample of Magnetite and Silica.

Magnetite from cones 3, 4 and 5 at 1.5, 1.5 and 2gms respectively were mixed with silica of equal cones at proportional mass ratios of 2, 4 and 6.

Another test was run using minus cone 5 at 5gm magnetite mixed with minus cone 5 silica mass ratios of 2, 4, and 6.

2.2.3 Variation of Flowrate.

To study the effect of flow rate variation on quality of separability minus cone 5 samples of 5gm of magnetite mixed with 25gm of silica were used. The tests run for each mixture were at 0.03, 0.06, 0.1, and 0.14 m/s..

2.2.4 Jarosite residue and Cottrell dust.

To further test the performance of the a.c. separator compared with the d.c. separator, jarosite residue and Cottrell dust samples from metallurgical plants were used.

For the jarosite residue and Cottrell dust, 40gm dry weight of the samples were suspended in 500ml water with 10gm of Calgonite added to effect dispersion. Each of the samples was placed in an ultrasonic bath to aid dispersion. The particle size of both samples was 80% minus cone 4. The tests run on both samples were carried out at flow rates of 0.03, 0.06, 0.1 and 0.14 m/s..

2.3 EXPERIMENTAL TECHNIQUE.

Three runs were carried out for every test. The flow rate was fixed at 0.03m/s for all the experiments, except for 2.2. and 2.3. In view of the inability to vary the a - c magnetic field strength, the field of 0.06tesla produced by the demagnetizing coil, was used in both a-c and d-c magnets.

The same sample presention system was used for both

magnets.

The procedure for each run was as follows:

a. The velocity through the matrix was set by placing the required velocity control plug in line.

b. The matrix and sample transporting line were filled with water.

c. A selected mass of sample was slurried and wetted by agitation in 250 cc of water.

d. The solenoid was switched on.

e. The on/off valves at the feed tank and below the matrix cannister were opened simultaneously. As the slurry passed through the matrix into a receiving bucket, water was added at the water tank to maintain a constant head.

f. When the discharge below the matrix was observed to be free of mineral particles the lower valve was closed.

g. The bucket was removed and replaced by another bucket.

h. The current was shut off, and three full velocity top and bottom flushes were applied to wash out the magnetic product into the mags bucket.

For the experiment with mechanical vibration, after step d, the vibrator was switched on, and before step f the vibrator was switched off.

For the minus cone 5 mixture samples, the jarosite residue and Cottrell dust, the fine matrix was used.

Before the beginning of every run, the entire transportation system and the matrix were flushed top and

bottom at full velocity twice.

Lastly the nonmagnetic and magnetic products were decanted, filtered, dried in an oven at 105 C and weighed.

2.4 ANALYSIS OF PRODUCTS.

For all the experiments two products were collected - a magnetic product (concentrate) consisting of particles captured on the matrix magnetically and physically entrapped nonmagnetic particles, and a nonmagnetic product (tailings) consisting of particles that passed through the magnetized matrix.

After weighing the two products, total losses were generally less than 1.5% but up to 9% for the jarosite residue and the Cottrell dust samples because of their extreme fineness.

For the synthetic samples (magetite/silica and magnetite/barytes) the grade of magnetic product was estimated from

$$\text{Grade} = \frac{\text{Mass of magnetite in feed}}{\text{Mass of magnetic product}} \qquad \text{eq.(52).}$$

since magnetite recovery was 100%. This estimate was checked by determining grade with the Davis tube (see Table 3). The difference is of the order of experimental repeatability.

The assaying of jarosite residue and Cottrell dust for both magnetic and nonmagnetic products was done by Atomic Absorption Spectrometry.

TABLE 3

COMPARISON OF GRADE

FOR MAGNETIC PRODUCT.

SILICA RATIO.	A S S A Y DAVIS TUBE Eq.(52)	FROM
	A. C. HGMS.	
	C O N E 4	
1	86.80	86.85
2	79.83	80.60
4	78.22	73.14
6	71.70	70.46
	D. C. HGMS.	
1	80.74	81.04
2	75.98	75.68
4	71.12	68.93
6	65.33	66.08

3 RESULTS

3.1 COMPARISON OF GRADE IN A.C. HGMS WITH D.C. HGMS.

Unless otherwise indicated, the results given are the average grade and range of the three runs presented as plots of grade, Gm, against the mass ratio of nonmagnetic to magnetic particles in the feed, A. The lines drawn are those of the void-filling model. Individual experimental data are given in appendix 1.

3.1.1 Equal Cone Mixtures.

The results are given in Figures 23,24,25, and 26 for cones 2,3,4, and 5 respectively. The grades for the a.c. separator were higher in every case. Also for both separators, the grades increased with decrease in cone size. On extension of the cone 2 sample mass ratio to 10 on the a.c. hgms Figure 27, there was no significant grade change observed. Figure 27a summarizes the results.

In Table 4 is shown the grade result for a mixture of magnetite-barytes compared to magnetite-silica separation in the a.c. magnetic separator.

With mixture ratio of 1 both grades were the same. For ratio 6, the grades of magnetic product for barytes were less than that of silica. However again the grades for cone 5 of the magnetite-barytes mixture were higher than for the cone 2 samples. This is in agreement with the results observed for the magnetite/silica samples.

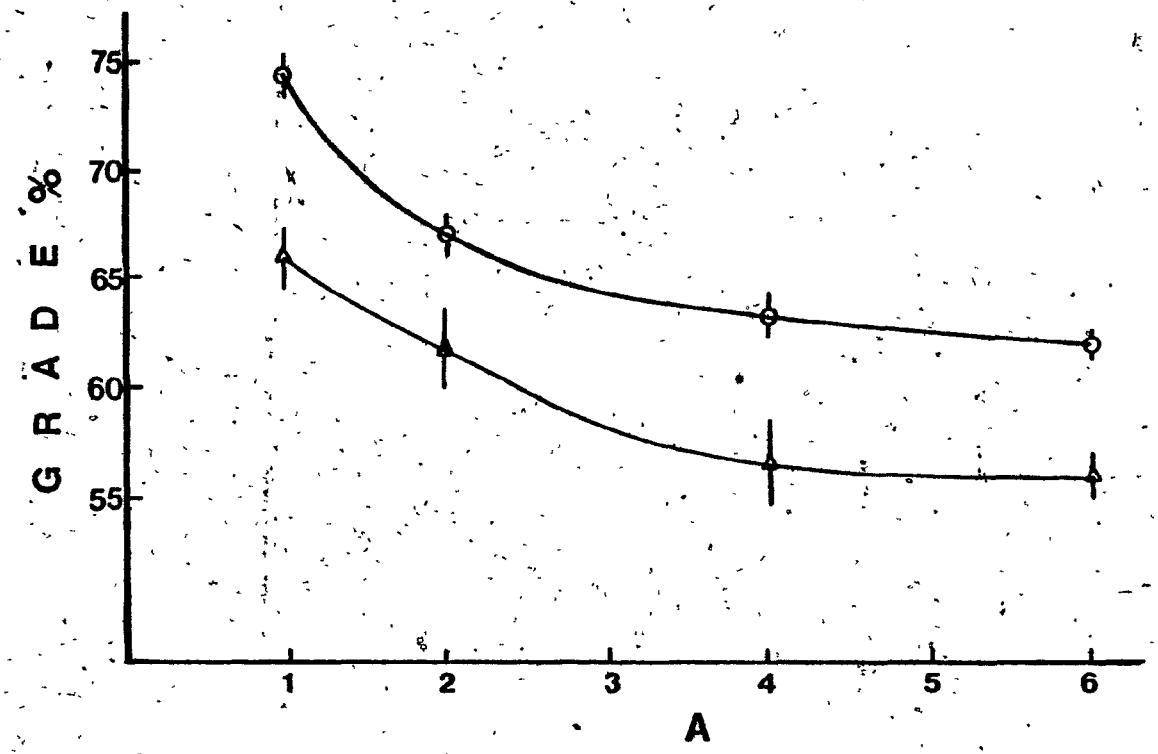

Figure 23 Comparison of average grade of magnetic product, Gm, for cone 2 in the a.c. hgms with d.c. hgms as to the mass ratio of silica to magnetite in the feed, A.

○ A.C. HGMS

Δ D.C. HGMS

The same symbols were used for all the graphs.

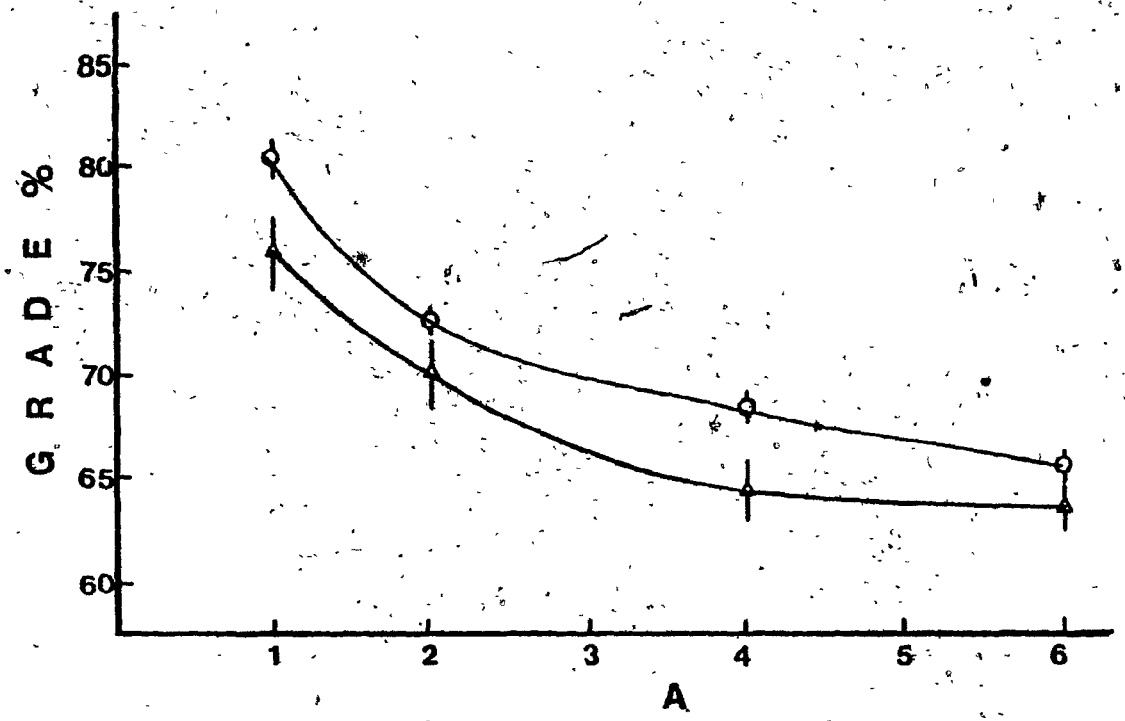

Figure 24 Comparison of average grade of magnetic product, Gm, for cone 3 in the a.c. hgms with d.c. hgms as to the mass ratio of silica to magnetite in the feed, A.

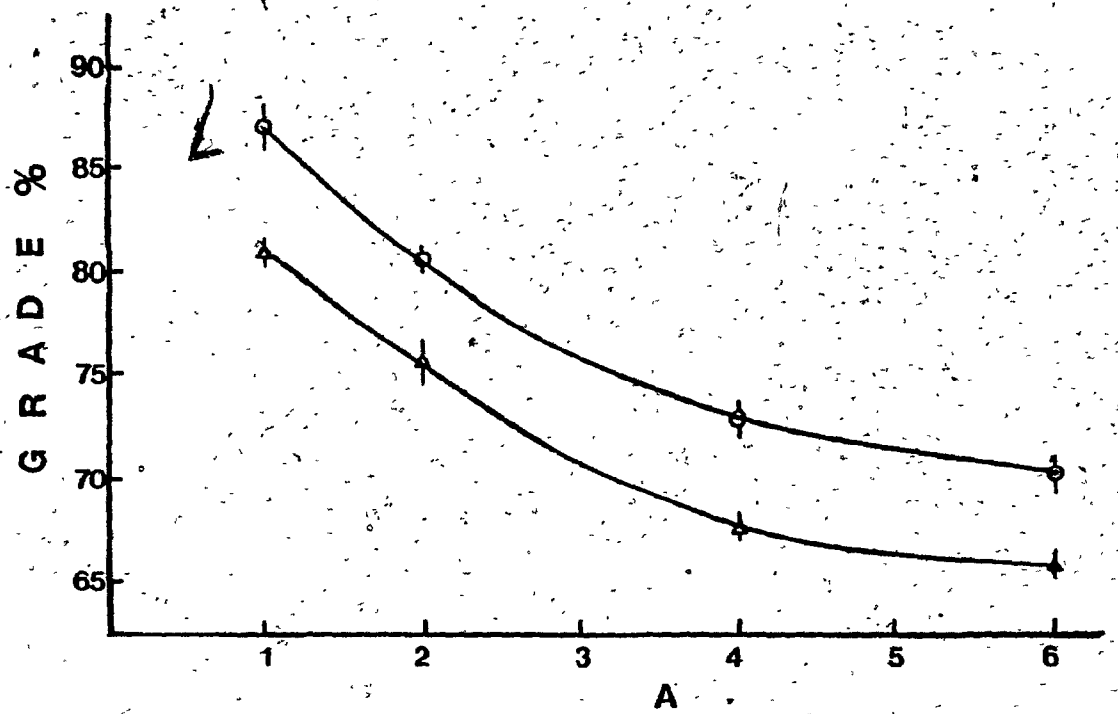

Figure 25 Comparison of average grade of magnetic product, Gm, for cone 4 in the a.c. hgms with d.c. hgms as to the mass ratio of silica to magnetite in the feed, A.

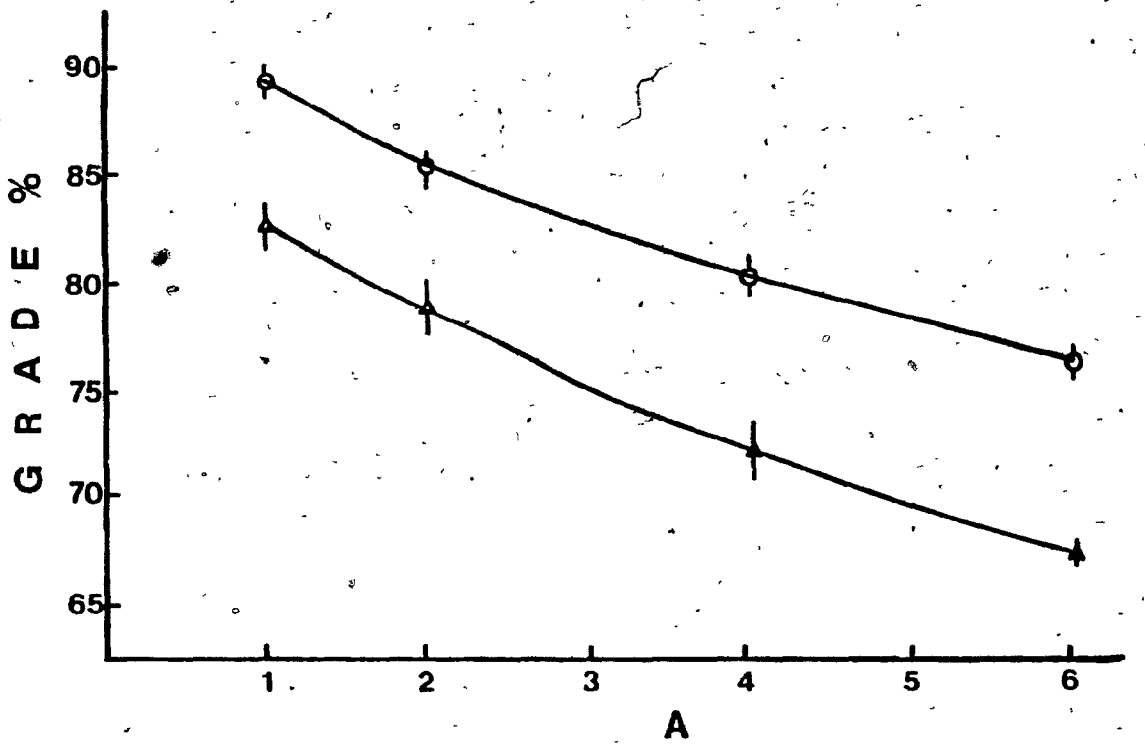

Figure 26 Comparison of average grade of magnetic product, Gm, for cone 5 in the a.c. hgms with d.c. hgms as to the mass ratio of silica to magnetite in the feed, A.

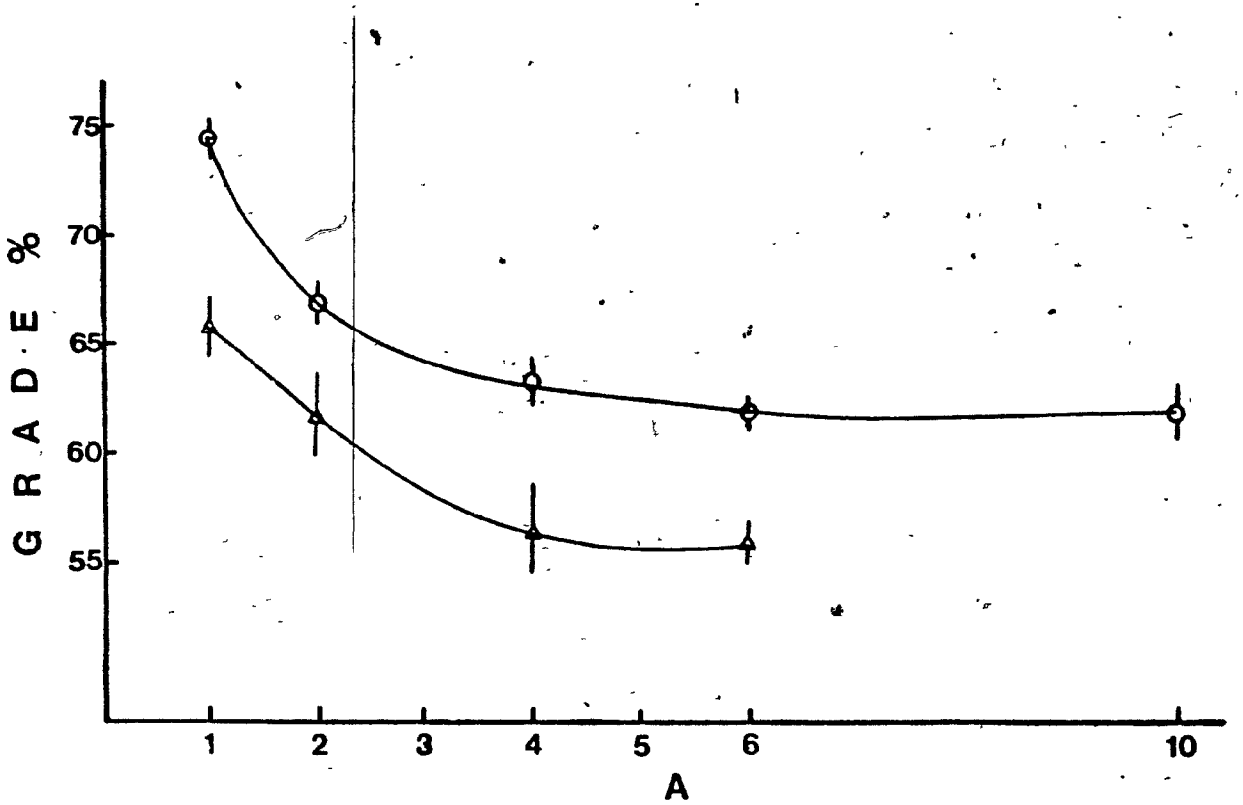

Figure 27 Plot of average grade of magnetic product, Gm, versus mass ratio of silica to magnetite in the feed, A - 10 for the a.c. hgms.

Figure 27a Plot of the overall result of average grade of magnetic product, Gm, versus mass ratio of silica to magnetite in the feed, A.

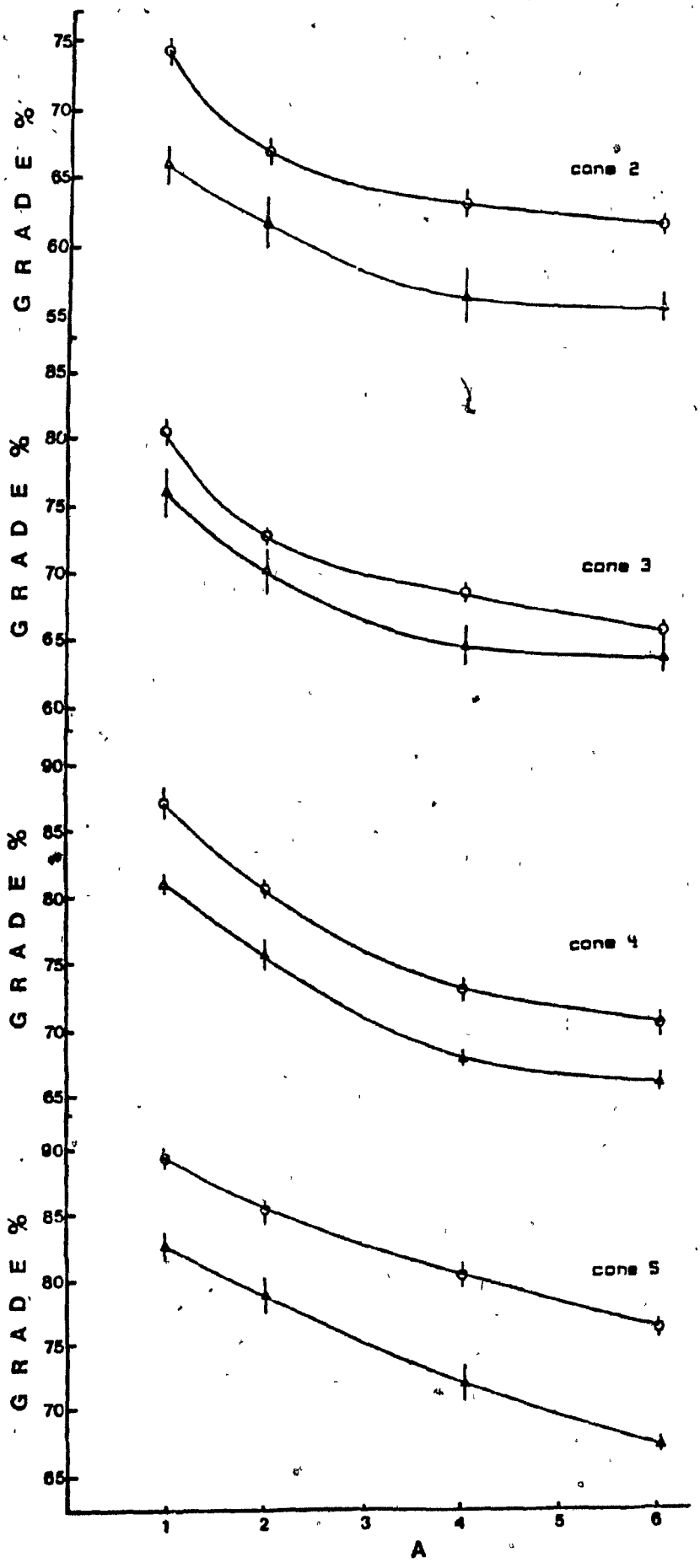
GRADE %
75
70
65
60
55
cone 2
GRADE %
85
80
75
70
65
60
cone 3
GRADE %
90
85
80
75
70
65
cone 4
GRADE %
90
85
80
75
70
65
cone 5
1
2
3
4
5
6
A

TABLE 4.

AVERAGE

PERCENT GRADE OF MAGNETIC PRODUCT

A.C. HGMS

RATIO	$BaSO_4$	SiO_2
	CONE 2	
1	75.99	74.55
6	53.46	62.21
	CONE 5	
1	90.69	82.69
6	69.41	67.45

3.1.2 Mixed Cone and minus Cone 5 Samples.

The comparison of grades for the a.c. hgms to that of d.c. Hgms are shown in Figures 28 and 29 respectively. The a.c. hgms gave higher grades than the d.c. hgms. Also the grade for minus Cone 5 was higher than the mixed cone sample.

The plots for the a.c. grades showed 'convex-like' shapes while for the d.c. the usual shape was observed.

3.1.3 Effect of Flowrate.

Increase of flow rate in both separators gave increase in grade, Figure 30. This was due to the cleaning action resulting from the increased drag force and because the force retaining the nonmagnetic particles is weak. Notwithstanding the a.c. hgms still maintained its higher grade product over that of d.c. hgms.

3.1.4 Effect of Mechanical Vibration in D.C. HGMS.

Figure 31 shows the result of separation using the d.c. hgms with a mechanical vibrator attached to the cannister compared to the regular a.c. and d.c. magnetic separators. A significant improvement in grade, up to 18%, was observed for separation with mechanical vibration.

3.1.5 Jarosite residue and Cottrell dust.

The results of Jarosite residue and Cottrell dust

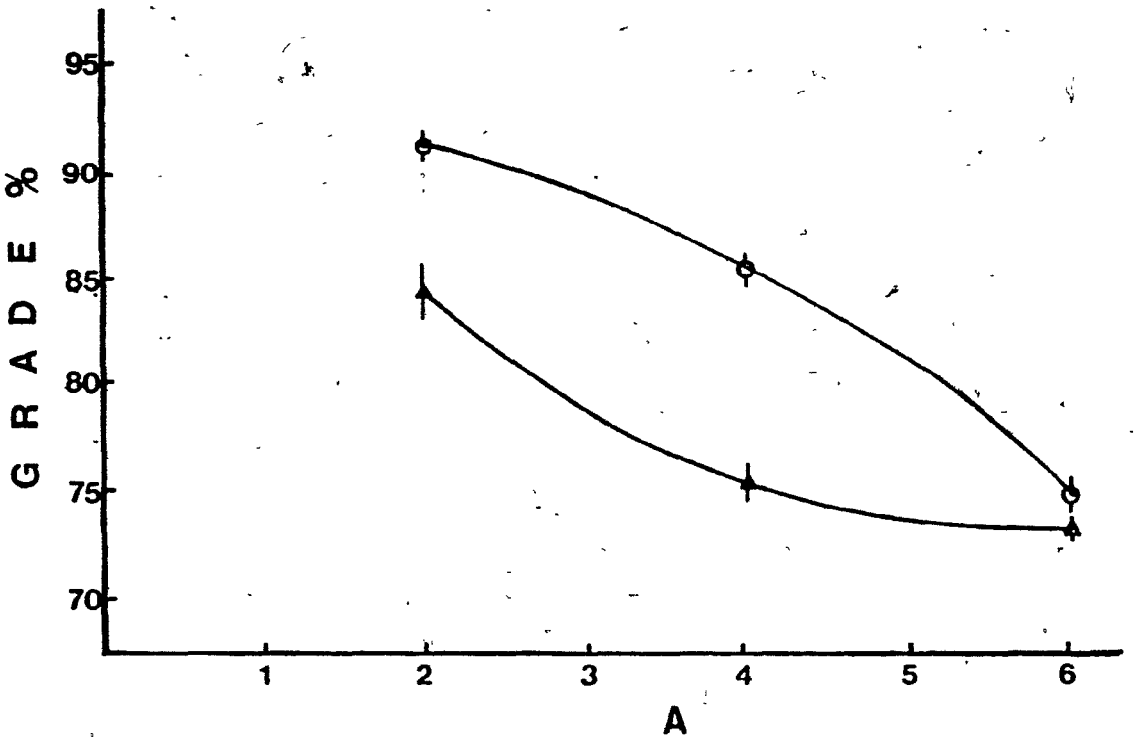

Figure 28 Comparison of average grade of magnetic product, Gm, for mixed cones 3, 4 and 5 in the a.c. hgms with the d.c. hgms as to the mass ratio of silica to magnetite in the feed, A.

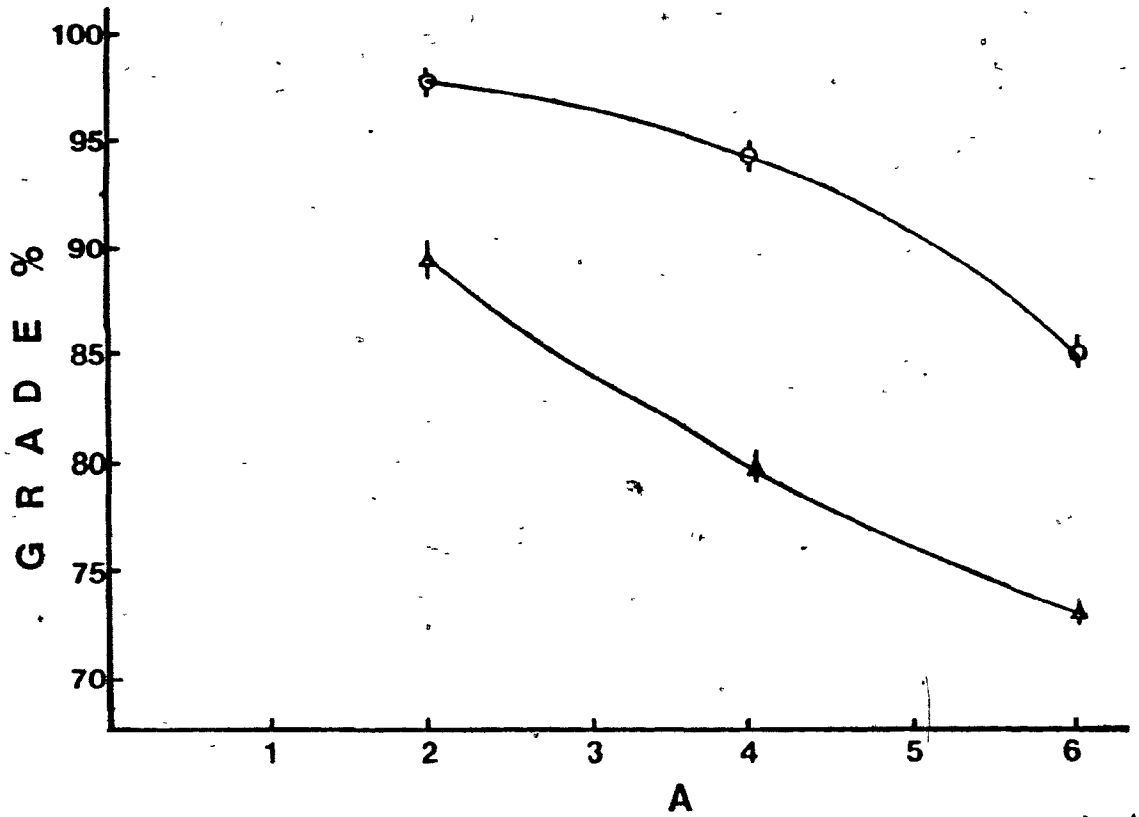

Figure 29 Comparison of average grade of magnetic product, Gm, for minus cone 5 in the a.c. with the d.c hgms as to the mass ratio of silica to magnetite in the feed, A.

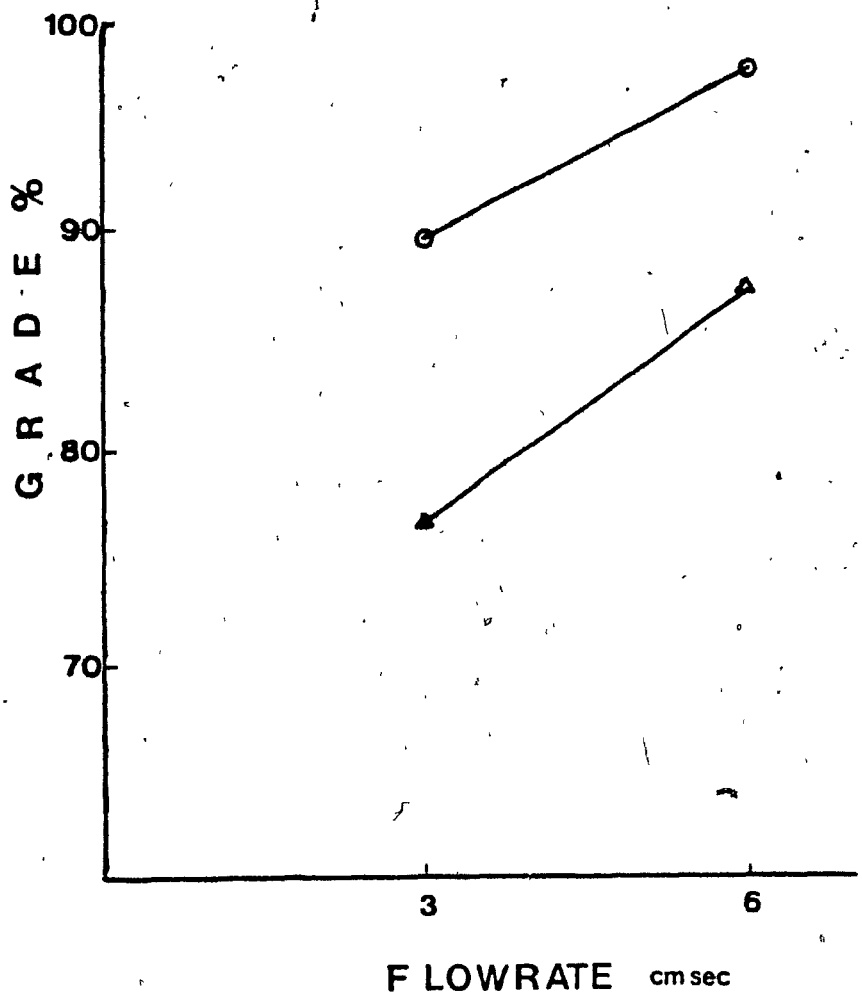

Figure 30 Comparison of grade of magnetic product, Gm, against flowrate variation for minus cone 5, in the a.c. hgms with the d.c. hgms at constant feed mass ratio of silica to magnetite 5:1. Data at 10 cm/sec. and above are not shown as magnetite recovery was less than 100%.

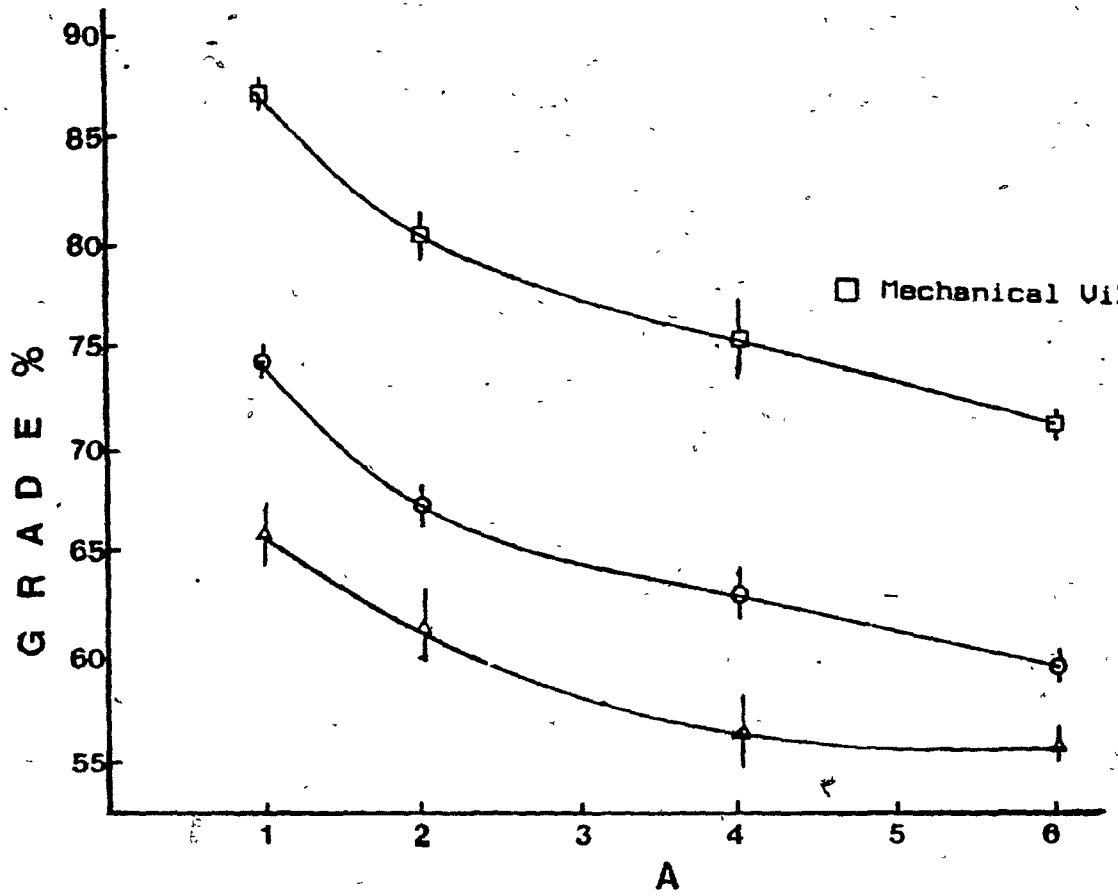

Figure 31 Comparison of average grade of magnetic product, Gm, for the mechanical vibration applied in the d.c. hgms with those of a.c. and d.c. hgms for cone 2 as to mass ratio of silica to magnetite in the feed, A.

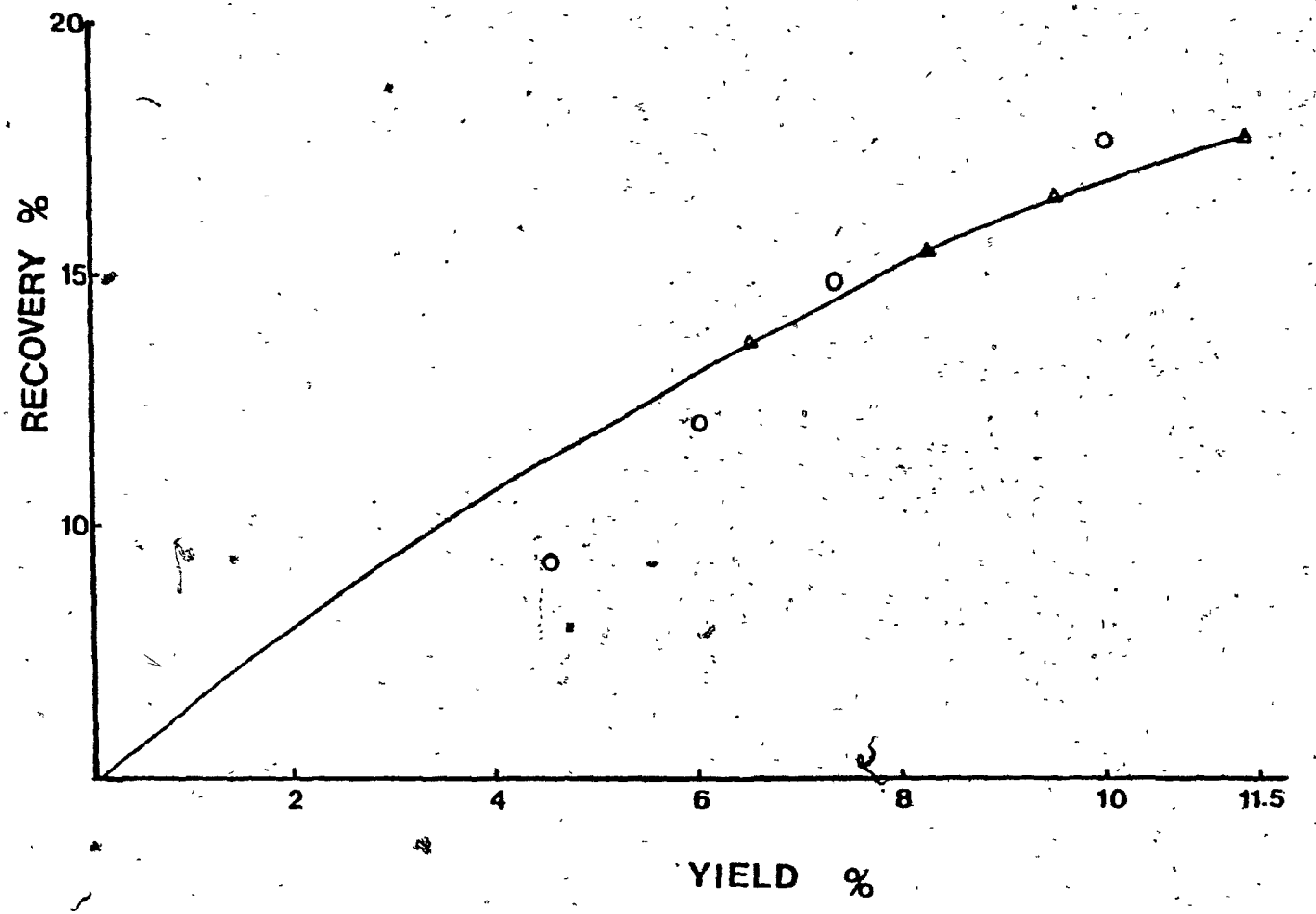

Figure 32 Jarosite residue Plot of recovery, R, of zinc, Zn, versus yield, Y, for the a.c. hgms and d.c. hgms.

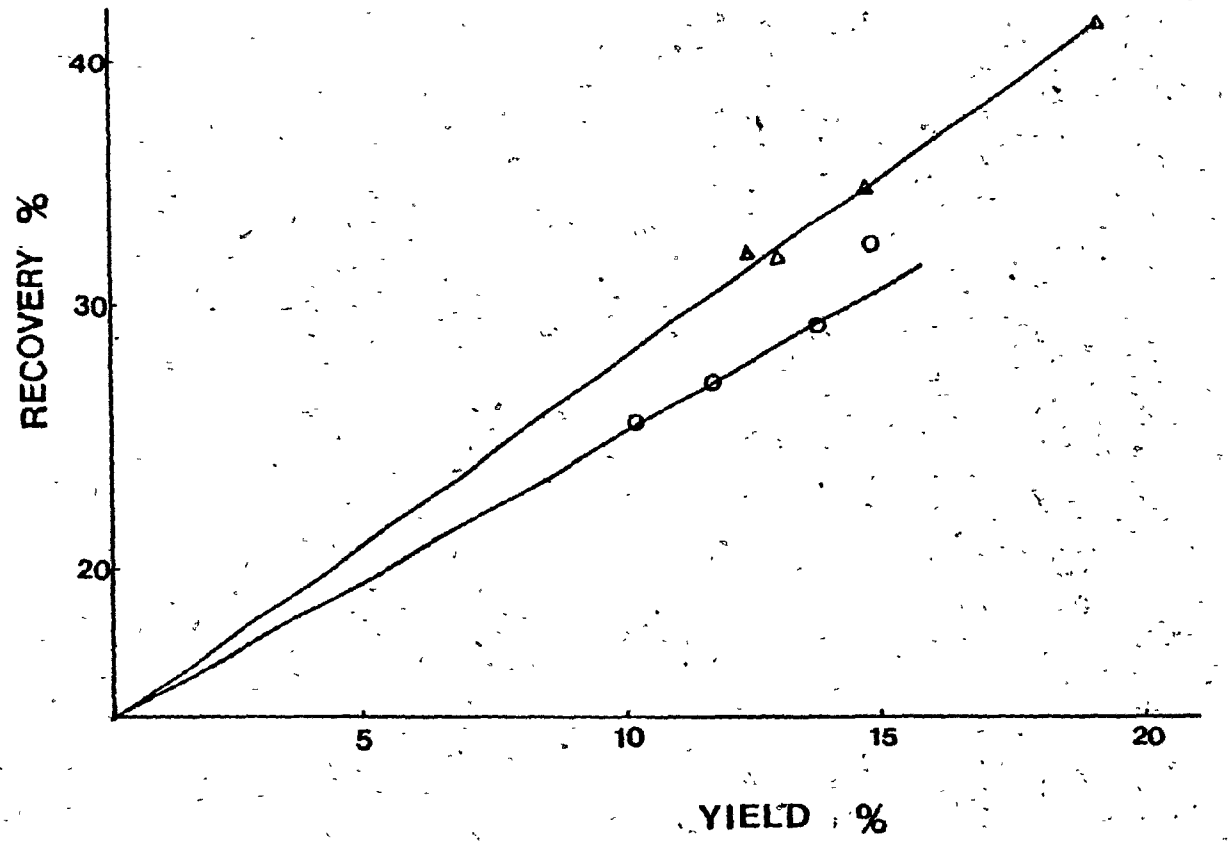

Figure 33 Cottrell dust Plot of recovery, R, of iron, Fe, versus yield, Y, for the a.c. hgms and d.c. hgms.

separation in the a.c. and d.c. separators are shown as plots of Recovery versus Yield in Figures 32 and 33 respectively. For both samples the best separation was achieved with the d.c. separator using the fine matrix.

3.2 TESTING THE GRADE MODELS

3.2.1 Oberteuffer Model

For the experimental conditions of this work, the ratio Fi/Fc in equation 33 can be assumed constant. Using equation 35, Figure 34 shows the plot of 1/Gm against A, for cone 2 of both the a.c. and d.c. hgms. Clearly the relationship is not linear and does not show a continuous decrease in grade as A increases as predicted by the equation.

3.2.2 Void-Filling Model

The estimated values of Vv and minimum grade are given in appendix 2. Vv is quite high (above 50%) which propably stems from the stringer formation being loosely packed (which is true by visual inspection). Using the data for cone 2 and 5 in equation (44), the results are shown as plots of ln (function) against A in Figures 35 and 36, respectively. The complete analysis and the values of a are given in appendix 3. The results of all the predicted grades compared with all the experimental average grades for are given in appendix 4.

In all the tested cases, the predicted values were in good aggrement with the experimental grades. The use of

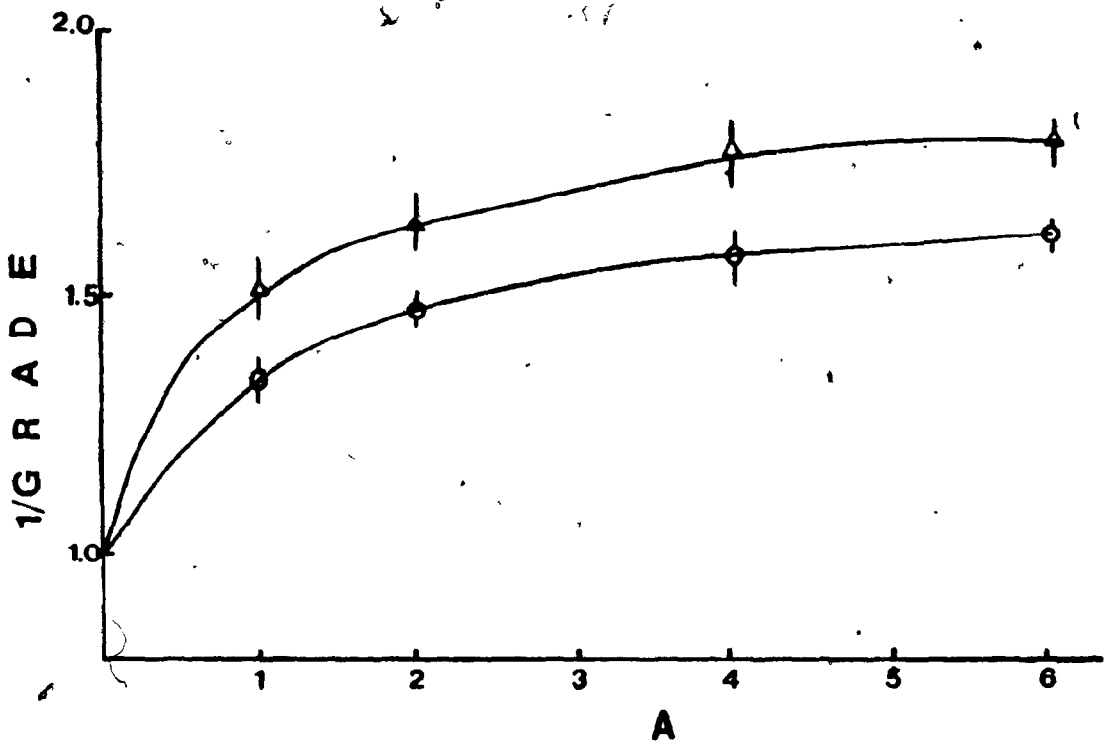

Figure 34 The plot of 1/Gm versus A, for cone 2 in the a.c. and d.c. hgms using Obertauffer model.

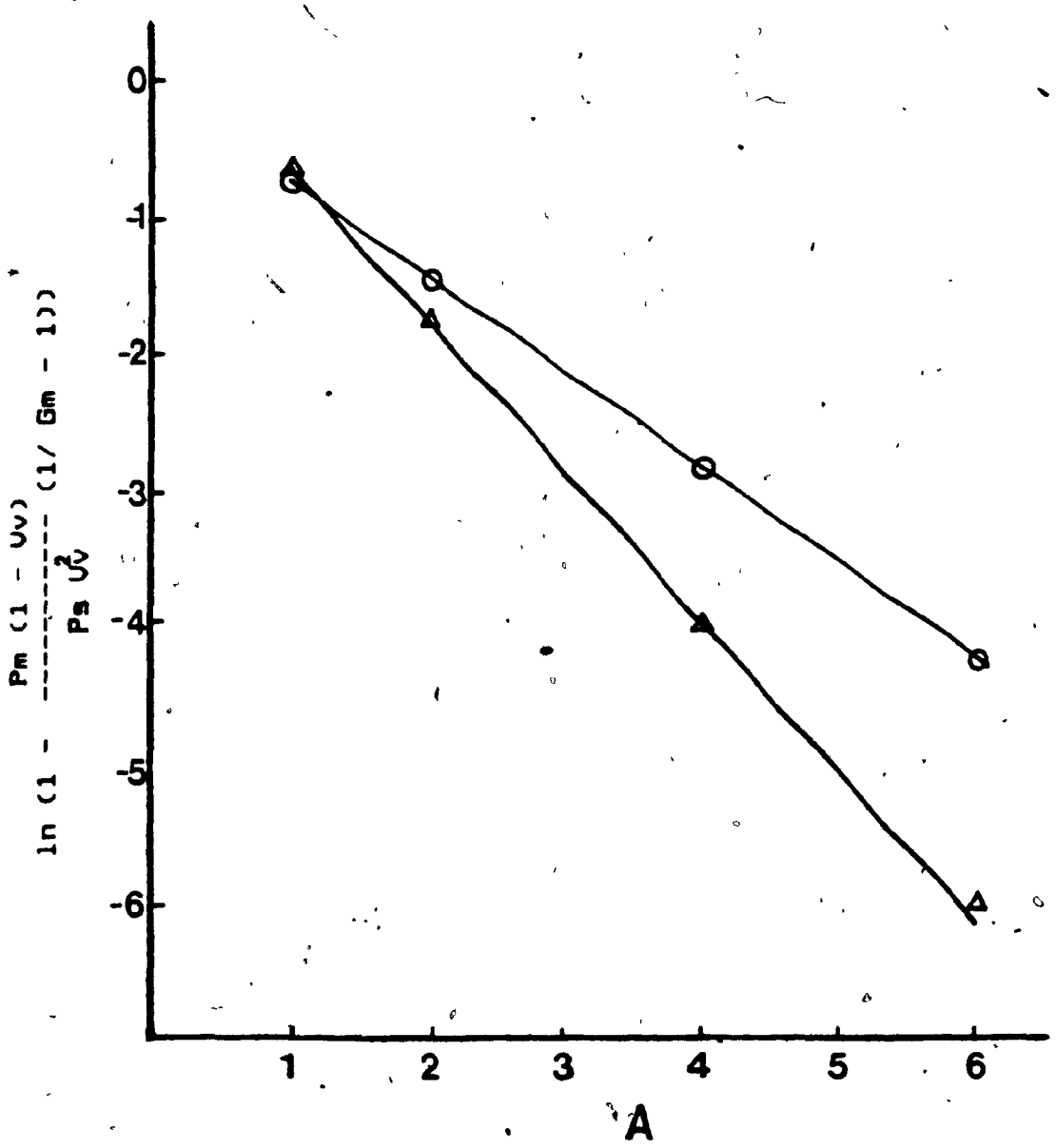

Figure 35 Plot of ln (function) versus A, for the a.c. and d.c. hgms for cone 2 sample.

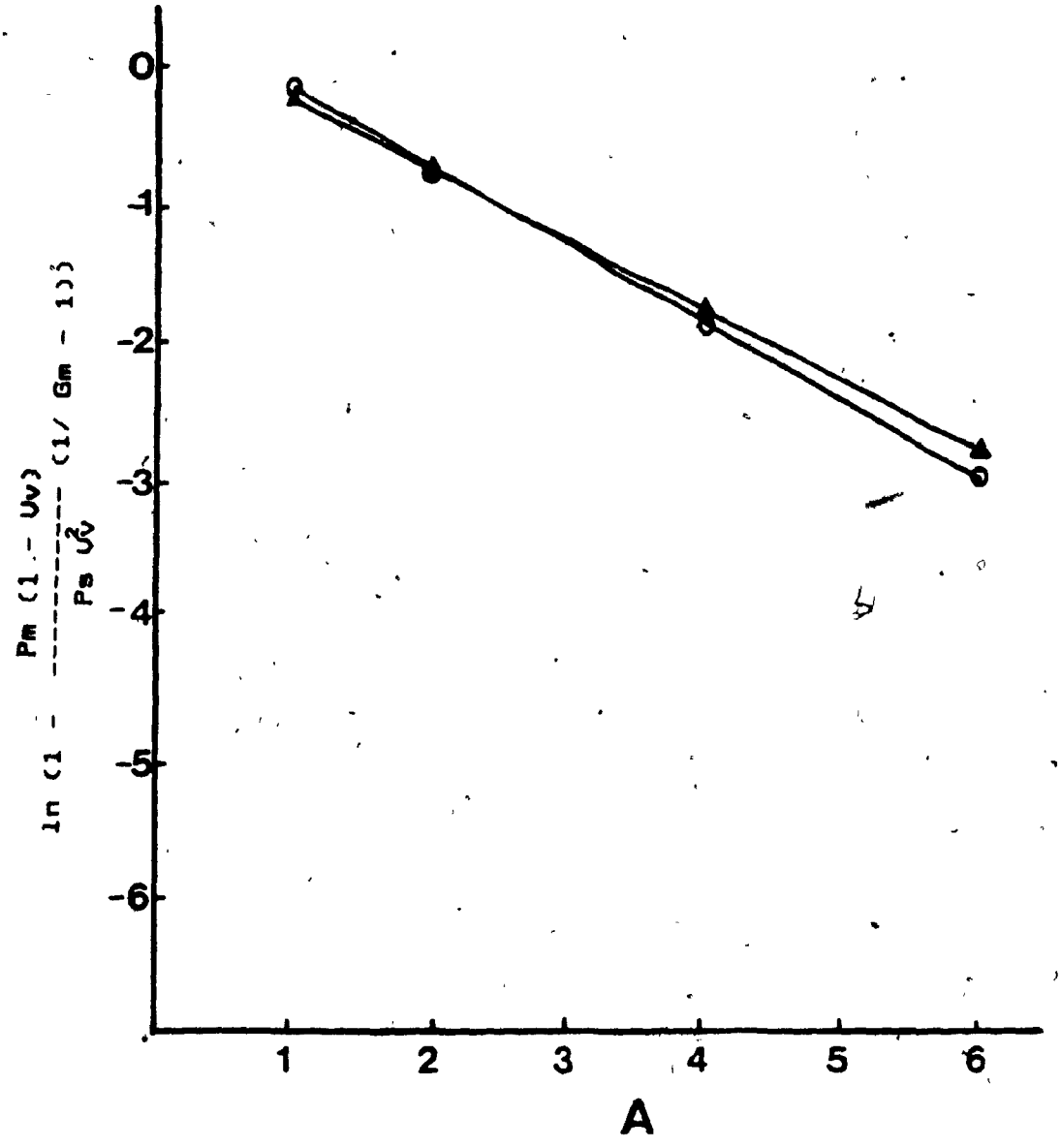

Figure 36 Plot of ln (function) versus A, for the a.c. and d.c. hgms for cone 5 sample.

mechanical vibration did not degrade the model fit.

Generally, the model predictions were satisfactory. To use the proposed model, experimental data must be generated on the sample/device combination to be used.

A major limitation is the assumption that the maximum fv is equal to Ov. There is no obvious reason why this should be. Other values of maximum fv are possible, for example, 1.0 or 0.74 the latter representing close packing. It is not possible to a-priori decide on the maximum fv. The assumption that void filling follows an exponential function is in line with the concept that the filling is a random process.

Like other models, this model will only be accepted when and after it stands the test using other mineral mixtures. The data on magnetite-barytes is not complete enough.

4 DISCUSSION

4.1 A.C. HGMS VERSUS D.C. HGMS.

The fact that the a.c.hgms captured magnetite particles proves that a net attractive magnetic force is exerted on the particle as suggested by the theoretical analysis (equation (19)).

For the equal cone samples the grades decreased exponentially and levelled off above about mass ratio 6. With the extension of the mass ratio to 10 for the cone 2 mixture for example, the grade remained the same. This suggested that there is a limit to the amount of silica that can be entrapped in the magnetic product.

The highest grades were observed for cone 5 while the lowest were for cone 2. This may be related to the decreased porosity associated with finer magnetite particles exposed to the same magnetic field, as reported in reference (32). Initial suspicion that this size effect may be related to the difference in particle size of magnetite and silica (due to method of sample preparation) was dispelled by the results with magnetite/barytes which showed the same size effect.

For mixed cone samples the shape of the curves for the d.c. hgms was the same as for the individual cone samples. However that of a.c. hgms was inverted. There is no immediate explanation for this difference; it is unlikely that this difference in shape has any important

significance. Again the highest grade product was achieved for separation in a - c hgms and for the finer size material (minus cone 5). The same reason (decreased porosity) given for the higher grade for equal cone mixture samples appears to remain valid for wide size ranges.

The higher grade of magnetic product for a.c. hgms versus d.c. hgms must be due to deflocculation or vibration effects. The experiments with d.c. hgms and mechanical vibration suggest that vibration is the dominant effect.

For the d.c. hgms with mechanical vibration the average grade of magnetic product improved by 10% over that of a.c. hgms and by 18% over that of d.c. hgms without vibration. This improvement confirms the effect and role of vibration during magnetic separation. For the a.c. solenoid hgms, vibration is produced by the varying magnetic force due to the alternating magnetic field acting both on the matrix and the particles.

Measurement of vibration in the a.c. hgms proved difficult since it is neccessary to measure the vibration of the magnetite bed, (the matrix is fixed and showed little vibration, Table 1). Experiments with magnetite fixed to the vibration sensor confirmed vibration. Certainly strong vibration is felt whenever magnetizable material is held by hand and brought into the a.c. hgms (with the d.c. solenoid hgms no vibration was experienced).

The vibration of the magnetic product presumably dislogdes some of the physically entrapped nonmagnetic

particles permitting them to be carried away by the hydrodynamic drag force. Thus, vibration is probably the cause of the higher grade of magnetic product using the a.c. hgms compared with the d.c. hgms observed in the magnetite-coal separation reported by Kelland et al (1).

These observations open the possibilty of vibration in magnetic separation. This work has shown that nonmagnetic particles physically entrapped in the magnetic product can be removed by vibration which reduces the need for re-cleaning. Vibration can be induced by using a.c. hgms but this will be restricted to relatively low fields. This work has shown that mechanical vibration can be used. This is convenient since it separates vibration from magnetic field production. Mechanical vibration should be usable on high field d.c. hgms, although installation may be difficult with continous hgms devices. Vibration could be mechanical (as here) or acoustic. Similar observations regarding vibration appear to have been reached concurrently by Sun et al (39). However there is insufficient data on the vibration, how it was created and quantified, for comparison with this work.

4.2 JAROSITE RESIDUE AND COTTRELL DUST.

The d.c. hgms showed a slight performance advantage over the a.c. hgms. However it is very difficult to attribute this performance to the type of magnet used. The recovery versus yield plots revealed little element separation was actually achieved. Apart from iron the

tendecy was more to splitting of the material rather than separation.

These two samples were thought to represent possible practical examples of mixtures of strongly magnetic phases (ferrites) with non-magnetic phases (e.g. lead sulphate) which could benefit from a.c. hgms. Subsequent analysis showed this was not the case. With jarosite, the sodium jarosite itself was only about 10 times less magnetic than the ferrite (40) and in the case of the Cottrell dust, phase interlocking essentially restricts physical separation (41).

5. CONCLUSIONS.

5.1 CONCLUSION.

1. That an a-c driven magnet can be used for magnetic separation.

2. For mixtures of fine magnetic and nonmagnetic particles, the a-c driven magnet gives superior grades (5 to 10 percent) over all tested conditions.

3. The grade of magnetic product for both a-c and d-c magnets a) decreases with increase in particle size, b) decreases with increase in ratio of nonmmagnetic to magnetic particles in the feed and c) increases with flowrate.

4. On application of an external vibration to the d-c driven magnet, the grade of magnetic product was improved up to 18 percent.

5. Entrapment of nonmagnetic particles in the magnetic product can be reduced by vibration.

6. A new model of simulating the grade of magnetic product based on 'void-filling' has been tested and found to fit the experimental results.

5.2 CLAIMS FOR ORIGINAL RESEARCH.

1. The magnetic force on a particle in a demagnetizing solenoid was derived. (This is original, to the best of the author's knowlegde).

2. An explanation based on vibration was forwarded to explain the improved grade of a.c. versus d.c. hgms observed here and by Kelland et al (1).

3. The application of external mechanical vibration during magnetic separation and its effect was examined.

4. A model of grade for magnetic product in high gradient magnetic separation was developed and tested.

5.3 SUGESSTIONS FOR FUTURE WORK.

1. A detailed study of the use and limits of vibration.

2. Test industrial/plant samples with application of vibration.

3. Work to further test the model of grade.

APPENDIX 1
TABLE 1.1.

AVERAGE

PERCENT GRADE OF MAGNETIC PRODUCT

SiO_2 RATIO	A.C. KGMS	D.C. KGMS
	CONE 2	
1	74.55	66.08
2	67.38	61.80
4	63.45	56.35
6	62.21	55.85
10	62.08	--.--
	CONE 3	
1	80.52	72.29
2	72.89	70.44
4	68.52	64.59
6	65.65	63.69

TABLE 1.1A.

INDIVIDUAL TEST RESULTS FOR

PERCENT GRADE OF MAGNETIC PRODUCT

SiO_2 RATIO	A.C. KGMS	D.C. KGMS
	CONE 2	
	74.18	62.57
1	74.85	68.78
	74.63	67.20
	68.12	58.07
2	67.75	63.86
	66.31	63.86
	63.05	51.97
4	64.85	58.07
	62.50	59.03
	61.88	56.43
6	61.73	56.50
	63.05	55.49
	61.50	--.--
10		
	62.66	--.--

TABLE 1.1B.

INDIVIDUAL TEST RESULTS FOR

PERCENT GRADE OF MAGNETIC PRODUCT

SiO_2 RATIO	A.C. HGMS	D.C. HGMS
	CONE 3	
	81.43	72.67
1	80.13	67.39
	80.00	76.80
	72.99	66.66
2	72.57	73.64
	73.10	76.80
	68.59	63.78
4	68.21	62.34
	68.78	67.66
	67.20	61.43
6	65.79	63.86
	64.02	65.79

TABLE 1.2.

A V E R A G E

PERCENT GRADE OF MAGNETIC PRODUCT

SiO_2 RATIO	A.C. KGMS	D.C. KGMS
	C O N E 4	
1	86.86	81.04
2	80.60	75.69
4	73.14	68.94
6	70.46	66.08
	C O N E 5	
1	89.55	82.69
2	85.52	78.95
4	80.56	72.22
6	76.61	67.45

TABLE 1.2A.

INDIVIDUAL TEST RESULTS FOR

PERCENT GRADE OF MAGNETIC PRODUCT

SiO_2 RATIO	A.C. KGMS	D.C. KGMS
	CONE 4	
	86.66	80.65
1	89.61	80.65
	87.72	81.83
	80.13	74.29
2	80.91	75.87
	80.78	76.92
	72.05	68.59
4	73.64	69.54
	73.75	68.68
	70.13	65.62
6	70.72	66.14
	70.52	66.49

TABLE 1.2B.

INDIVIDUAL TEST RESULTS FOR

PERCENT GRADE OF MAGNETIC PRODUCT

SiO_2 RATIO	A.C. KGMS	D.C. KGMS
	C O N E S	
	89.13	83.89
1	90.42	83.33
	89.13	81.43
	86.66	77.40
2	84.32	78.25
	85.62	81.30
	80.65	70.42
4	79.49	72.15
	81.57	74.18
	76.92	67.57
6	76.80	67.29
	76.10	67.48

TABLE 1.3

INDIVIDUAL TEST RESULTS FOR

PERCENT GRADE OF MAGNETIC PRODUCT

A.C. HGMS

RATIO	$BaSO_4$	SiO_2
	CONE 2	
	76.69	74.18
1	75.64	74.85
	75.64	74.63
	52.69	61.88
6	53.82	61.73
	53.88	63.05
	CONE 5	
	90.25	89.13
1	91.07	90.42
	90.74	89.13
	69.54	67.57
6	69.44	67.29
	69.25	67.48

TABLE 1.4.

A V E R A G E

PERCENT GRADE OF MAGNETIC PRODUCT

SiO_2 RATIO	A.C. HGMS	D.C. HGMS
	MIXED CONES (3,4+5)	
2	91.21	82.27
4	85.43	75.57
6	84.99	73.54
	MINUS C O N E S	
2	94.21	88.45
4	91.74	79.74
6	87.89	76.99

TABLE 1.4A.

INDIVIDUAL TEST RESULTS FOR

PERCENT GRADE OF MAGNETIC PRODUCT

SiO_2 RATIO	A.C. HGMS	D.C. HGMS
	MIXED CONE (3,4+5)	
	94.46	84.27
2	94.21	82.27
	93.95	80.26
	85.11	77.42
4	85.43	75.57
	85.74	75.71
	85.57	73.26
6	84.99	73.54
	84.41	73.82

TABLE 1.48.

INDIVIDUAL TEST RESULTS FOR

PERCENT GRADE OF MAGNETIC PRODUCT

SiO_2 RATIO	A.C. HGMS	D.C. HGMS
	MINUS CONE 5	
	98.07	89.38
2	97.43	87.66
	97.50	88.30
	91.61	80.02
4	91.79	79.62
	91.81	79.52
	89.23	77.34
6	88.77	77.87
	88.72	77.75

TABLE 1.5.

VARIATION OF FLOWRATE EFFECT AVE-

RAGE PERCENT GRADE OF MAGNETIC PRODUCT

FLOWRATE cm/sec.	A.C. KGMS SiO_2. Fe_3O_4, S 1	D.C. KGMS
	MINUS	CONE S
3	89.73	77.03
6	97.48	87.41

TABLE 1.5A

VARIATION OF FLOWRATE EFFECT INDIV-

IDUAL PERCENT GRADE OF MAGNETIC PRODUCT

FLOWRATE cm/sec.	A.C. HGMS $SiO_2 : Fe_3O_4$, S 1.	D.C. HGMS
	MINUS	CONE S
	89.69	76.98
3	89.77	77.04
	89.72	77.07
	97.45	87.38
6	97.47	87.41
	97.51	87.44

TABLE 1.6.

AVERAGE

PERCENT GRADE OF MAGETIC PRODUCT

SiO_2 RATIO	(VIB) D.C. HGMS	A.C. HGMS	D.C. HGMS
	C O N E 2		
1	87.34	74.55	66.08
2	79.95	67.39	61.80
4	75.49	63.45	56.35
6	71.23	62.21	55.85

TABLE 1.6A.

INDIVIDUAL TEST RESULTS FOR

PERCENT GRADE OF MAGNETIC PRODUCT

SiO_2 RATIO	A.C. HGMS	D.C. HGMS
	(VIB.) C O N E 2	
	--	87.26
1		
	--	87.41
	--	79.37
2		
	--	80.52
	--	74.52
4		
	--	76.45
	--	71.33
6		
	--	71.12

TABLE 1.7.

REPRESENTATIVE

RESULTS ON JAROSITE RESIDUE.

FLOWRATE cm/sec.	YIELD (%)	RECOVERY % ZINC	GRADE OF ZINC (%)
	D. C. HGMS		
3	11.36	17.70	11.29
6	9.48	16.47	12.59
10	8.25	15.10	13.35
14	6.48	13.71	15.32
	A. C. HGMS		
3	9.97	17.56	12.75
6	7.73	14.82	13.88
10	5.99	11.96	14.45
14	4.58	9.17	14.50

TABLE 1.7A.

RESULTS ON JAROSITE RESIDUE.

FLOWRATE cm/sec.	YIELD (%) D. C.	GRADE OF ZINC (%) HGMS.
	11.54	---
3	11.36	11.29
	11.42	---
	9.63	---
6	9.48	12.59
	9.75	---
	8.19	---
10	8.25	13.35
	8.12	---
	6.49	---
14	6.48	15.32
	6.50	---

TABLE1.7B

RESULTS ON JAROSITE RESIDUE.

FLOWRATE cm/sec.	YIELD (%)	GRADE OF ZINC (%)
	A. C.	HGMS.
	9.78	---
3	9.97	12.75
	9.88	---
	7.62	---
6	7.73	13.88
	7.52	---
	5.80	---
10	5.99	14.45
	5.65	---
	4.55	---
14	4.58	14.50
	4.52	---

TABLE 1.8

REPRESENTATIVE

RESULTS ON COTTRELL DUST

FLOWRATE cm/sec.	YIELD (%)	RECOVERY % IRON	GRADE OF IRON (%)
	D. C. HGMS		
3	18.48	40.94	13.18
6	14.56	34.94	14.28
10	12.89	32.06	14.80
14	12.32	32.09	15.5
	A. C. HGMS		
3	14.74	32.55	13.14
6	13.60	29.37	12.85
10	11.60	26.92	14.25
14	10.09	25.61	15.10

TABLE 1.8A.

RESULTS ON COTTRELL DUST

FLOWRATE cm/sec.	YIELD (%) D.C.	GRADE OF IRON (%) HGMS.
	18.23	---
3	18.48	13.18
	18.15	---
	14.25	---
6	14.56	14.28
	14.41	---
	12.82	---
10	12.89	14.80
	12.73	---
	12.35	---
14	12.32	15.5
	12.30	---

TABLE 1.8B.

RESULTS ON COTTRELL DUST

FLOWRATE cm/sec.	YIELD (%) A.C.	GRADE OF IRON (%) HGMS.
3	14.62	---
	14.74	13.14
	14.54	---
6	13.85	---
	13.60	12.85
	13.79	---
10	11.51	---
	11.24	14.25
	11.27	---
14	9.89	---
	10.09	15.10
	9.91	---

APPENDIX 2

TABLE 2.1.

COMPARISON OF AVERAGE PERCENT MINIMUM GRADE OF MAGS. PRODUCT FOR EQ.(39) OF THE MODEL WITH OBSERVED

VOL. OF VOIDS	A.C. PREDICTED	A.C. OBSERVED	MGMS
	CONE 2		
.655	61.7	62.2	
	CONE 3		
.63	65.1	65.7	
	CONE 4		
.59	70.2	70.5	
	CONE 5		
.54	75.9	76.6	
	MIXED CONE 3,4,5		
.45	84.5	85.0	
	MINUS CONE 5		
.41	87.5	84.9	

TABLE 2.2.

COMPARISON OF AVERAGE PERCENT MINIMUM GRADE OF MAGS. PRODUCT FOR EQ.(39) OF THE MODEL WITH OBSERVED

VOL. OF VOIDS	D.C. PREDICTED	HGMS OBSERVED
	CONE 2	
.695	55.8	55.8
	CONE 3	
.65	62.4	63.6
	CONE 4	
.625	65.8	66.1
	CONE 5	
.62	66.4	67.5
	MIXED CONE 3,4,5	
.57	72.6	73.5
	MINUS CONE 5	
.53	76.9	77.0
	MECH. VIB. CONE 2	
.59	70.2	71.2

APPENDIX 3

TABLE 3.1.

THE VALUES OF THE SLOPE, a, FROM THE PLOT OF EQUATION (44) OF THE PROPOSED MODEL

SiO_2 RATIO	$\ln\left(1 + \frac{Pm\ (1 - \upsilon v)}{Ps\ \upsilon^2}\ (1/Gm - 1)\right)$	
	A.C. HGMS	D.C. HGMS
FOR a = 0.8, r = .99, s = 0.06		
FOR a = 1.1, r = .99, s = 0.36		
	C O N E 2	
1	0.85	0.73
2	1.44	1.82
4	2.85	4.02
6	4.25	6.21
	C O N E 3	
FOR a = 0.6, r = .98, s = 0.31		
FOR a = 0.75, r = .96, s = 0.21		
1	0.51	0.97
2	1.11	1.38
4	2.31	2.2
6	3.51	3.02

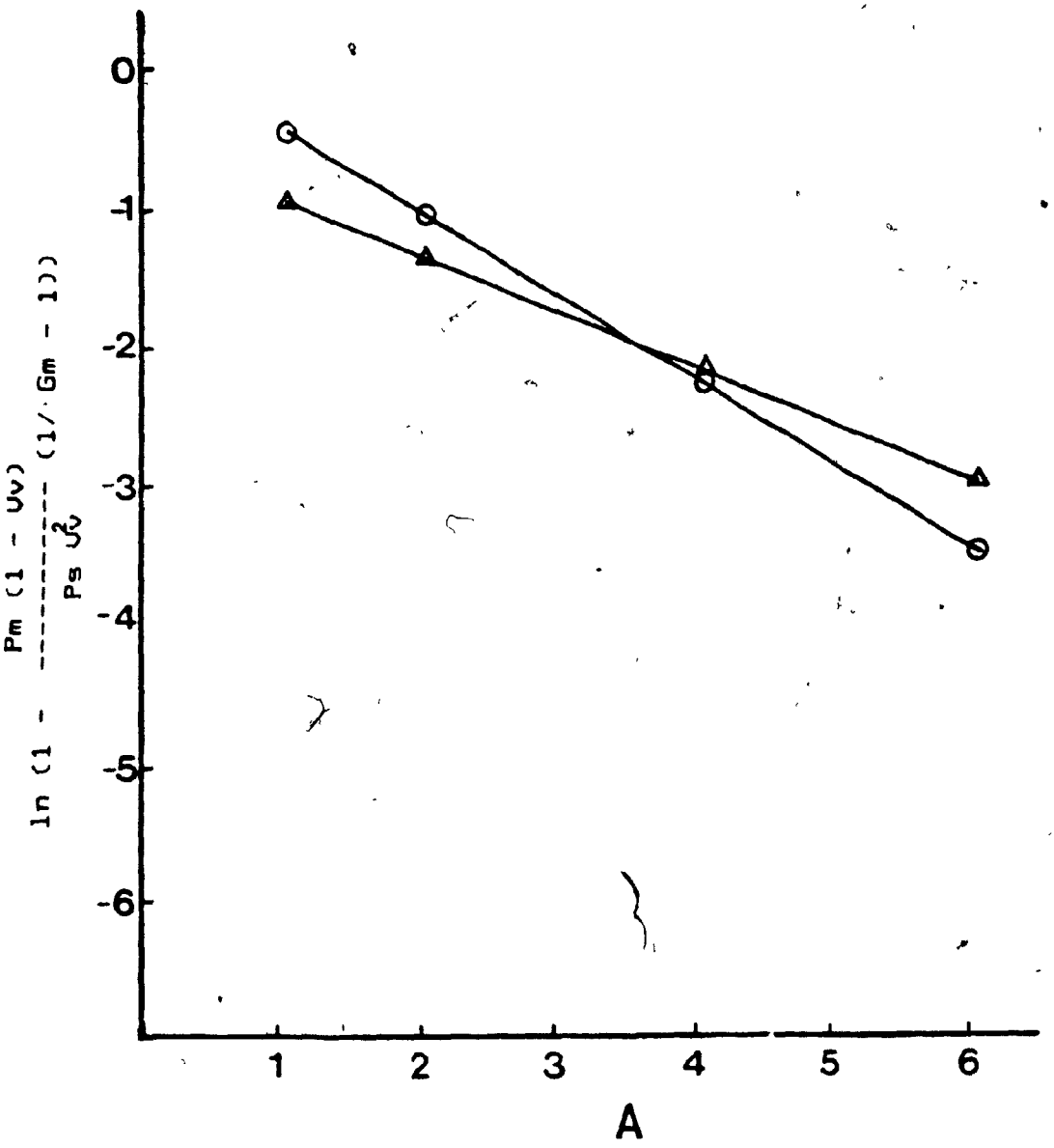

Figure 37 Plot of ln (function) versus A, for the a.c. and d.c. hgms for cone 3 sample.

TABLE 3.2.

THE VALUES OF THE SLOPE, a, FROM THE PLOT OF EQUATION (44) OF THE PROPOSED MODEL

SiO_2 RATIO $\ln\left(1 - \frac{Pm\,(1 - \upsilon v)}{Ps\,\upsilon^2}\,(1/Gm - 1)\right)$	A.C. HGMS	D.C. HGMS
FOR a = 0.54, r = .98, s = 0.47		
FOR a = 0.7, r = .99, s = 0.25		
	C O N E 4	
1	0.44	0.39
2	0.84	1.13
4	2.00	2.61
6	4.4	4.1
	C O N E 5	
FOR a = 0.55, r = .96, s = 0.41		
FOR a = 0.53, r = .97, s = 0.37		
1	0.24	0.32
2	0.80	0.82
4	1.91	1.83
6	3.01	2.83

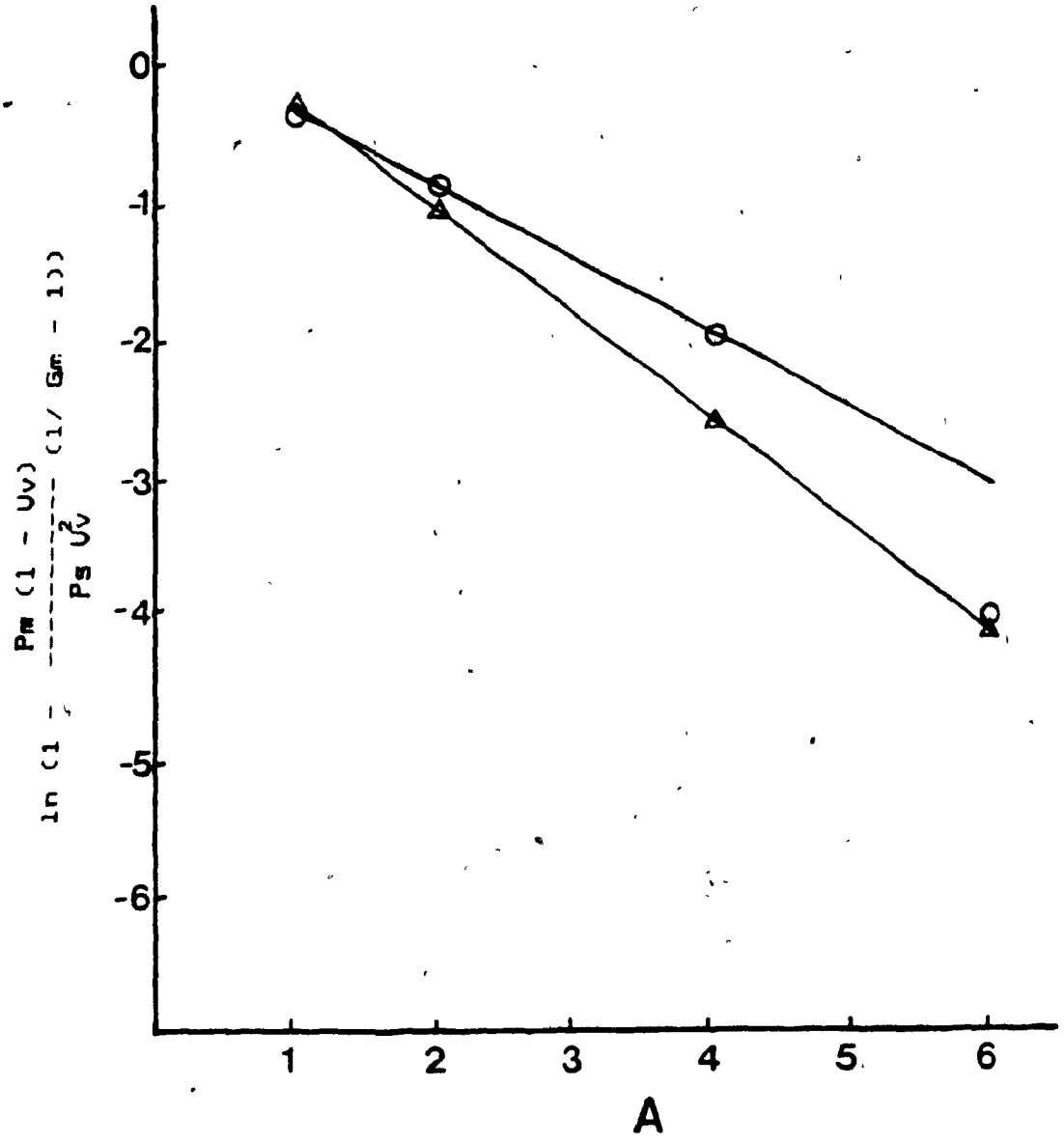

Figure 38 Plot of ln (function) versus A, for the a.c. and d.c. hgms for cone 4 sample.

TABLE 3.3.

THE VALUES OF THE SLOPE, a, FROM THE PLOT OF EQUATION (54) OF THE PROPOSED MODEL

SiO_2 RATIO	$\ln\left(1 - \frac{Pm\,(1 - Uv)}{Ps\,Uv^3}(1/Gm - 1)\right)$

	A.C. HGMS	D.C. HGMS
FOR a =0.61, r = .95, s =.51		
FOR a =0.55, r = .99, s = 0.00		
	MIXED CONES 3,4,5	
2	0.95	0.84
4	2.18	1.94
6	3.47	3.04
	MINUS C O N E 5	
FOR a = 0.7, r = .93, s = 0.88		
FOR a =0.66, r = .95, s = 1.22		
2	0.22	0.46
4	1.4	1.62
6	3.02	5.77

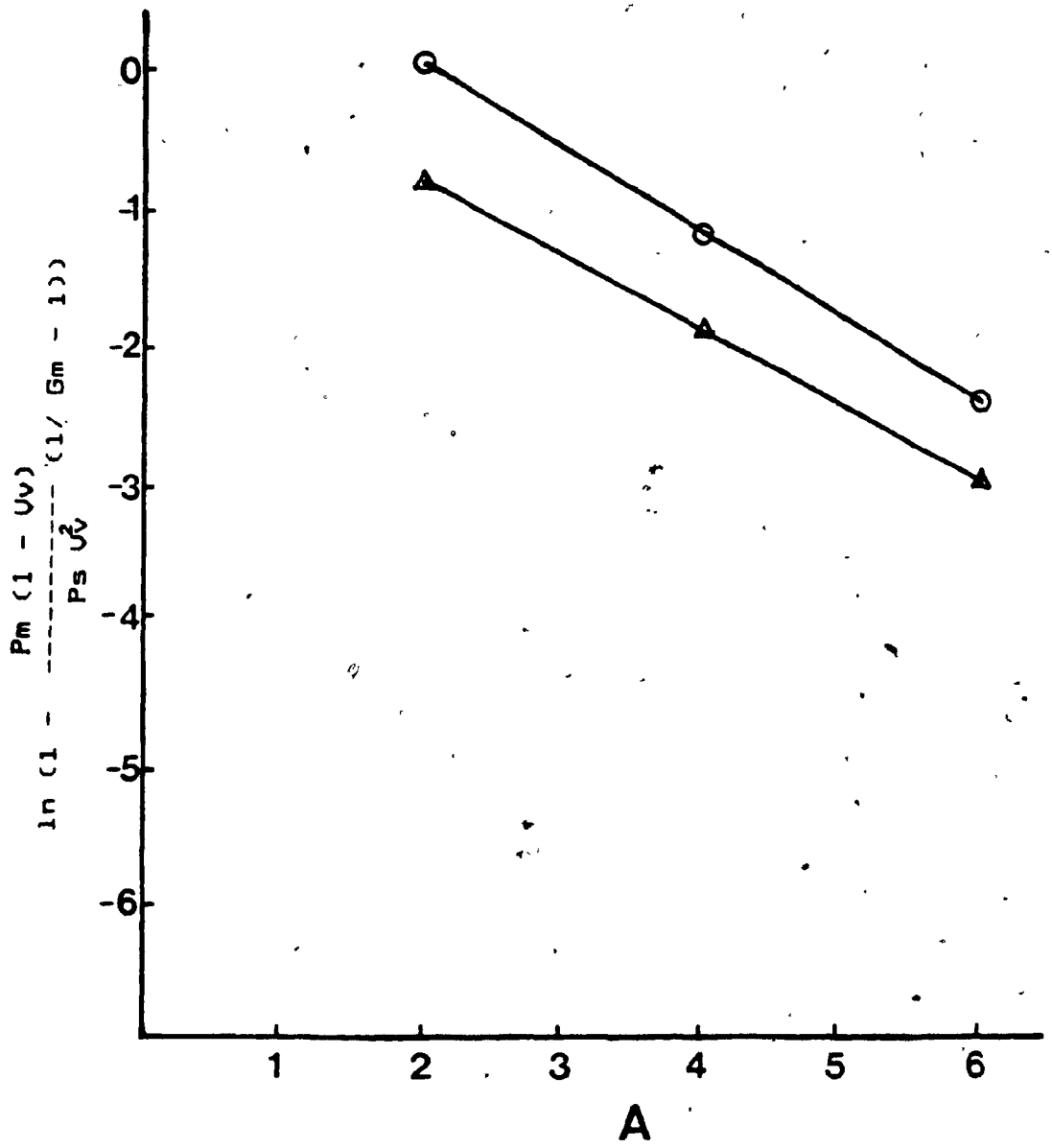

Figure 39 Plot of ln (function) versus A, for the a.c. and d.c. hgms for mixed cones 3,4&5 sample.

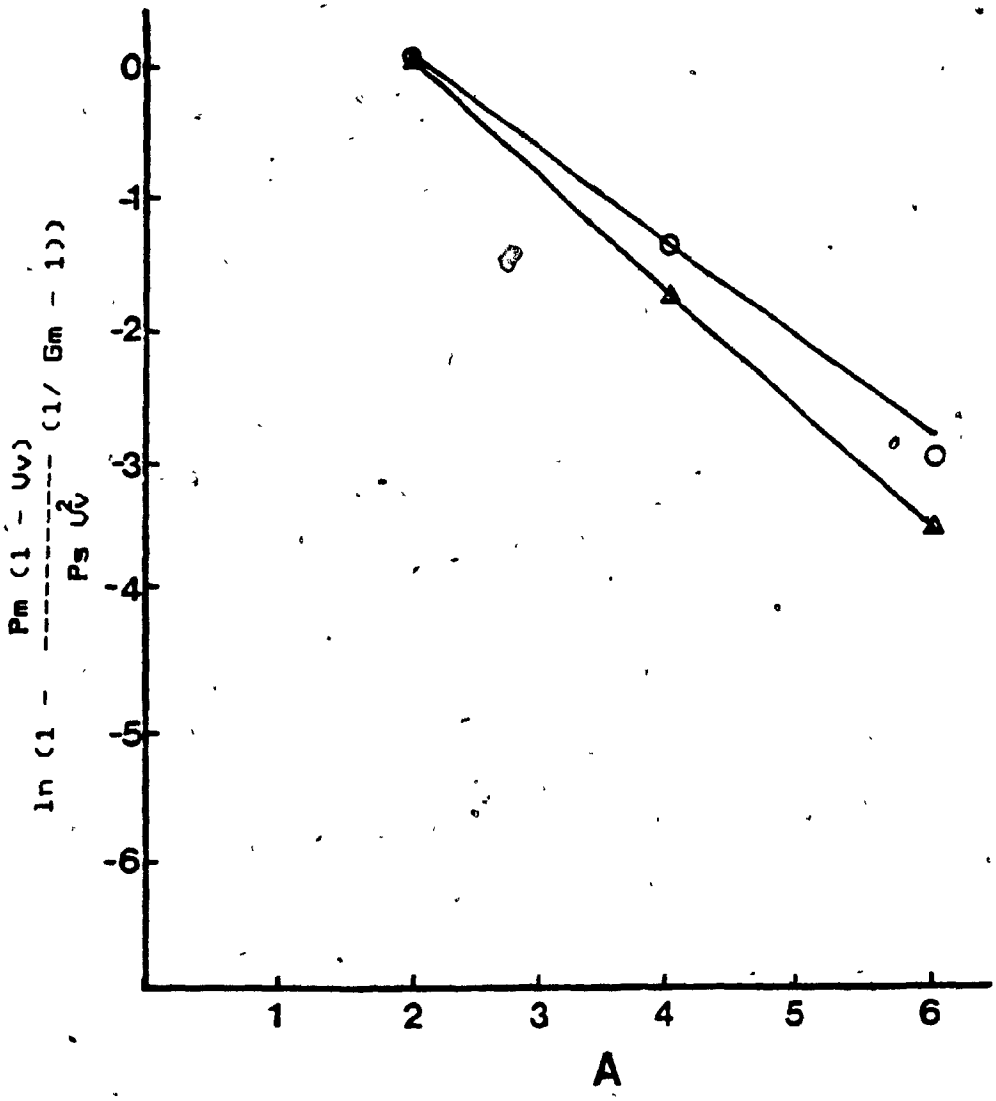

Figure 40 Plot of ln (function) versus A, for the s.c. and d.c. hgms for minus cone 5 sample.

TABLE 3.4.

THE VALUES OF THE SLOPE, a, FROM THE PLOT OF EQUATION (44) OF THE PROPOSED MODEL

SiO_2 RATIO	$\ln\left(1 - \frac{Pm\,(1 - Uv)}{Ps\,Uv^2}(1/Gm - 1)\right)$	
	A.C. HGMS	D.C. HGMS
FOR a = 0.5, r = .97, s = 0.31		
	MECH. VIBR.	C O N E 2
1	----	0.33
2	----	0.82
4	----	1.82
6	----	2.82

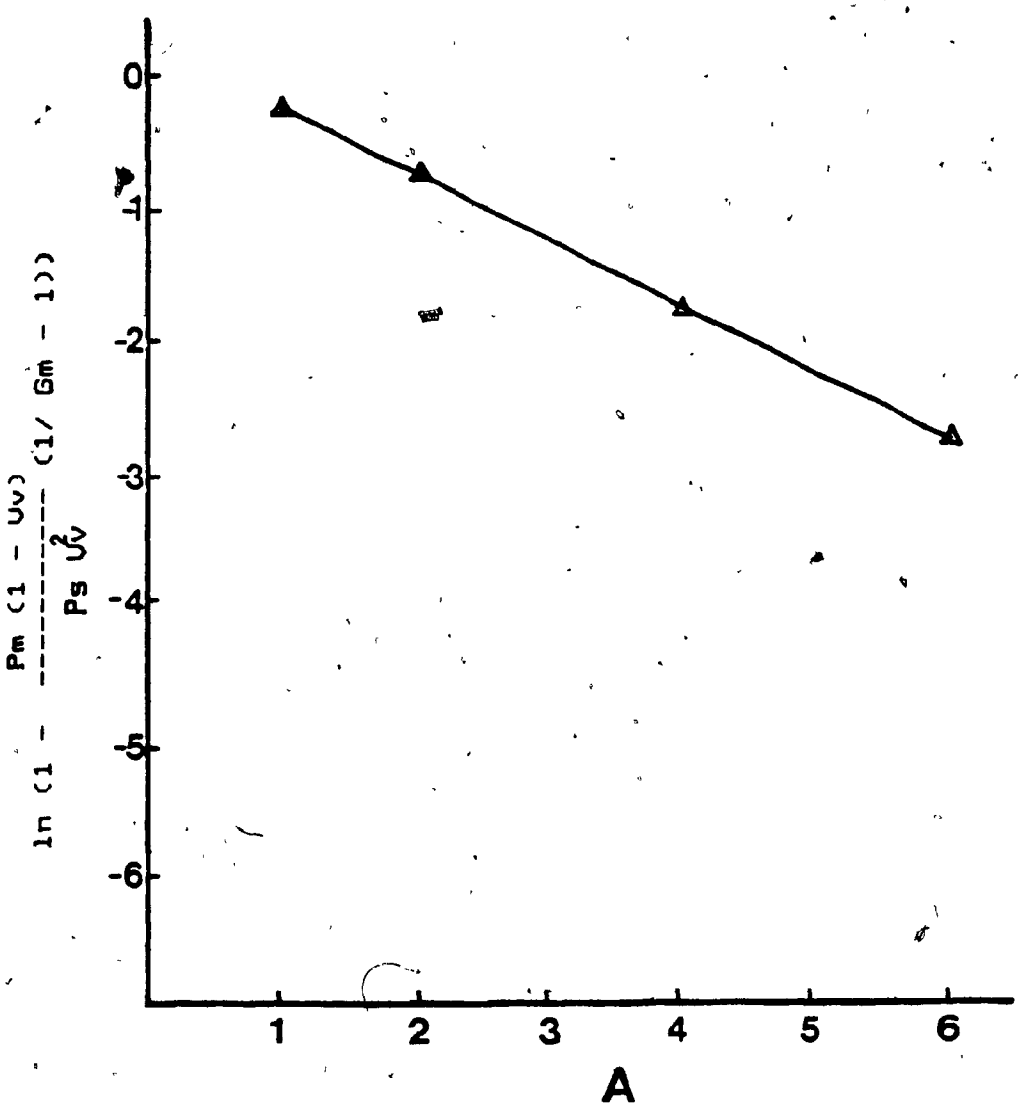

Figure 41 Plot of ln (function) versus A, for the d.c. hgms with mechanical vibrator attached for cone 2 sample.

APPENDIX 4

TABLE 4.A.

COMPARISON OF AVERAGE PERCENT GRADE OF MAGNETIC PRODUCT FOR THE PROPOSED MODEL WITH OBSERVED.

SiO_2 RATIO	A.C.	HGMS
	PREDICTED	OBSERVED
	C O N E 2	
1	74.5	74.6
2	66.8	67.4
4	62.6	63.5
6	61.9	62.2
10	61.7	62.08
	C O N E 3	
1	80.5	80.5
2	72.7	72.9
4	67.2	68.5
6	65.7	65.7

TABLE 4.B.

COMPARISON OF AVERAGE PERCENT GRADE OF MAGNETIC PRODUCT FOR THE PROPOSED MODEL WITH OBSERVED.

SiO_2 RATIO	D. C. HGMS	
	PREDICTED	OBSERVED
	CONE 2	
1	65.4	66.1
2	58.7	61.8
4	56.1	56.4
6	55.8	55.9
	CONE 3	
1	75.8	72.1
2	68.1	70.3
4	63.6	64.5
6	62.6	63.6

TABLE 4.1A.

COMPARISON OF AVERAGE PERCENT GRADE OF MAGNETIC PRODUCT FOR THE PROPOSED MODEL WITH OBSERVED.

SiO_2 RATIO	A.C. HGMS	
	PREDICTED	OBSERVED
	CONE 4	
1	85.0	86.9
2	78.1	80.6
4	72.7	73.1
6	71.0	70.5
	CONE 5	
1	88.2	89.6
2	82.5	85.5
4	78.0	80.6
6	76.6	76.6

TABLE 4.1B.

COMPARISON OF AVERAGE PERCENT GRADE OF MAGNETIC PRODUCT FOR THE PROPOSED MODEL WITH OBSERVED.

SiO_2 RATIO	D. C.	HGMS
	PREDICTED	OBSERVED
	CONE 4	
1	79.2	81.0
2	71.8	75.7
4	67.2	67.8
6	66.1	66.1
	CONE 5	
1	82.8	82.7
2	75.2	79.0
4	69.2	72.2
6	67.4	67.5

TABLE 4.2

COMPARISON OF AVERAGE PERCENT GRADE OF MAGNETIC PRODUCT FOR THE PROPOSED MODEL WITH OBSERVED.

SiO_2 RATIO	D.C. HGMS	
	PREDICTED	OBSERVED
WITH MECH. VIBRATION (CONE 2)		
1	85.7	87.3
2	78.8	80.0
4	73.1	75.5
6	71.3	71.2

TABLE 4.3

COMPARISON OF AVERAGE PERCENT GRADE OF MAGNETIC PRODUCT FOR THE PROPOSED MODEL WITH OBSERVED.

SiO_2 RATIO	A.C. PREDICTED	HGMS OBSERVED
	MIXED CONES 3,4,5	
2	88.6	91.2
4	85.7	85.4
6	84.8	85.0
	MINUS CO N E 5	
2	90.3	94.2
4	88.2	91.7
6	87.7	87.9

TABLE 4.3A.

COMPARISON OF AVERAGE PERCENT GRADE OF MAGNETIC PRODUCT FOR THE PROPOSED MODEL WITH OBSERVED.

SiO_2 RATIO	D.C. / HGMS	
	PREDICTED	OBSERVED
	MIXED CONES 3,4,5	
2	79.9	82.3
4	74.9	75.6
6	73.1	73.5
	MINUS CONES	
2	82.7	88.4
4	78.6	79.7
6	77.0	77.0

REFERENCES.

1.- Kelland, D.R., Dobby, G.S. and Maxwell, E., "Efficient HGMS for Highly Magnetic Material", IEEE Trans. Mag., MAG-17, No.6 (1981) 3308.

2.- Wells, P.F., "Report of Falconbrigde concentrator", internal report, Falconbrigde Limited.

3.- Liu, Y.A. and Lin, C.J., "Assessment of Sulfur and Ash Removal from Coals by Magnetic Separation", IEEE Trans. Mag., MAG-12, No.5 (1976) 538.

4.- Fleming, I.K., Smith, C.J. and Hoban, M., "Optimising the usage of magnetite at a mordern coal prepeation plant", Aus. I.M.M. Confr., (Sept.,1982) 361.

5.- Iannicelli, J., "Paramagnetic Separation in Ultrafine Industrial Minerals and Coal",AIME/SME Annual Meeting, Atlanta,Georgia, (3, 1983) 6-10.

6.- Clark, G., "Industrial Mineral Processing", 4-Magetic Separation (May,1985) 21-33.

7.- Oder, R.R., "High Gradient Magnetic Separation, Theory and Applications", IEEE Trans. Mag., MAG-12, No.5 (1976) 428.

8.- Price, C.R. and Abercrombie, W.F., "Industrial Applications of Magnetic Separation", IEEE Pub. No.78CH1447-2MAG, N.Y. (1979) 14.

9.- Jones, G.H., " The Separation of Strongly Magnetic Particles Particularly Those of Small

Dimension", Proc.7th IMPC., I.M.M., London (1964) 405.

10.- Anon. Report on Mount Pleasant Mine, Mining Magazine (July,1983) 16-61.

11.- Oberteuffer, J.A. and Wechsler, I., "Fine Particles Processing", Ed. Somasundaran, P., N.Y. (1980) 1178

12.- Malghan, S.G. and Van Dillen, J.P., "Influence of Process Variables in the High Gradient Separation of Uranium Ores", Min. Engr., (Dec.,1984) 1650.

13.- Corrans, I.J., Gilbert, W.A., Lindell, K.S. and Dunne, R.C., "The Performance of an Industrial Wet High-Intensity Magnetic Separator for the Recovery of Gold", Journ. of SAIMM (3,1984) 57.

14.- Espinosa-Gomez, R., M.Eng. Thesis, McGill Univ., Montreal, (1982).

15.- Trindade, S.C. and Kolm, H.H., "Magnetic Desulfurization of Coal",IEEE Trans. Mag., MAG-9, No.3 (1983) 310.

16.- Hall, S.T., Ph.D. Thesis, McGill Univ., Montreal, (1985).

17.- Melville, D., Paul, F. and Roath, S., "Red Blood Cells in High Gradient Magnetic Separation", IEEE Trans. Mag., MAG-11, No.6 (1975) 1701.

18.- de Latour, C. and Kolm, H., "Magnetic Separation in Water Pollution Controll-II", IEEE

Trans. Mag, MAG-11, No.5 (1975) 1570.

19.- Heitman, H.G., "Studies of the Application of Electromagnetic Filters in Power Plants", IEEE Pub. No.78CH1447-2MAG, N.Y. (1979) 115.

20.- Obertueffer, J.A., "Magnetic Separation A review of principles, Devices and Applications" IEEE Trans Mag, MAG-10, No.2 (1974) 223.

21.- Lawver, J.E. and Hopstock, D.M., "Wet Magnetic Separation of Weakly Magnetic Minerals", Min. Sci. Engng. 6 (3), (1974) 154.

22.- Jone, G.H., British Patent No.768,451 (1975)

23.- Jones, G. H., "Wet Magnetic Separator for Feebly Magnetic Minerals", Proc. 5th IMPC., Inst. of Min. and Metall., London (1963) 717.

24.- Stone, W.J., ibid., p.733.

25.- Kolm, H.H., Obertueffer, J.A. and Kelland, D.R., "High-Gradient Magnetic Separation", Scientific American 233 (5), (Nov., 1975) 46.

26.- U.S. Patent No.3,627,678 (1971).

27.- U.S. Patent No.3,920,543 (1975).

28.- Finch, J.A., "Magetic Sepration", Seminar held at McGill Univ., (1984).

29.- Stekly, Z.J.J., "A Superconducting High Intensity Magnetic Separator",IEEE Trans. Mag, MAG-11, No.5 (1975) 1594.

30.- Winch, P.R., "Electricity and Magnetism". 2nd.

Edition, Englewood Cliff, N.J. (1963) 378.

31.- Lomovtsev, L.A. and Schugol, L.S., "The Effect of Magnetic Flocculation on Magnetic Concentration Process", (In Russian) Gorn. Jurn., No.8 (1967) 56.

32.- Eyssa, Y.M. and Boom, R.W., "Magnetic and Coagulation Forces on a Suspension of Magnetic Particled", Inter. Journ. of Min. Proc., No.3 (1976) 1-8.

33.- Benson, W.H., Bartnik, J.A. and Rose, G.D., "Demagnetizing Coils and Magnetic Flocculators Used in Magnetite Beneficiation", Mining Engng. (1968) 130

34.- Lantto, Hekki, "The Effect of Magnetic Flocculation in the Beneficiation of Magnetic Materials", Acta Poly. Scan., Chp133, UDC.622.778:537.624, Helsinki, (1977).

35.- Hartig, H.E., Onstad, N.I. and Foot, N.S., "Demagnetization of Magnetite", Univ. of Minnesota, Mines Experiment Station, Inf. Circ. No.7, (May,1951).

36.- U.S. Patent No.1,286,247 (Dec.,1918).

37.- Williams, M.F. and Hendrickson, L.G., "Depolarizing Magnetite Pulps", Trans. AIME, Min. Engng., (Feb.,1956) 201.

38.- Kesall, D.F. and McAdam, J.C.H., "Design and

Operating Characteristics of a Hydraulic Cyclone Elutraitor", Trans. Inst. Chem. Eng. Vol. 41 (1963) 84-95

39.- Sun Zhongyuan and Li Zhengnan, "A Study of Vibration High Gradient Magnetic Separation", Proc.25th IMPC., Cannes, (June,1985) TOME 1, 140

40.- Hall, S.T., Rao, S.R., Goodluck, O. and Finch, J.A. "Some Applications of Magnetic Separation in Fine Particle Processing", presented ta the 16th Annual Meeting of Fine Particle Society, Miami, April.

41.- Castra-Quintero, R., Rowlands, N., Rao, S.R. and Finch, J.A., "Characterization and Separation of a Cu-Smelter Dust Residue", submitted for publication, Canadian Metallurgical Quarterly.